Environmental Modelling and Software 198 (2026) 106896

Contents lists available at ScienceDirect

Environmental Modelling and Software

journal homepage: www.elsevier.com/locate/envsoft

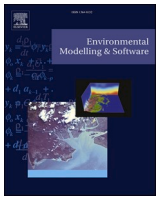

Modeling hydrologic response to wildfires in the Pacific Northwest with a modified calibration technique

Hyunwoo Kang [a,c,*], Cameron E. Naficy [b,c], Kevin D. Bladon [c,d]

[a] Department of Civil and Environmental Engineering, Washington State University, Pullman, WA, USA
[b] Pacific Northwest Region, USDA Forest Service, Baker City, OR, USA
[c] Department of Forest Ecosystems and Society, College of Forestry, Oregon State University, Corvallis, OR, USA
[d] Department of Forest Engineering, Resources, and Management, College of Forestry, Oregon State University, Corvallis, OR, USA

ARTICLE INFO

Keywords:
Wildfire
Hydrology
SWAT
Calibration
Streamflow
Evapotranspiration
Fire severity
Water balance

ABSTRACT

The 2020 Labor Day fires in the Western Cascades of Oregon, USA, burned extensive forested areas, which altered hydrologic processes, water quality, aquatic ecosystems, and drinking water resources. Understanding wildfire severity effects on hydrologic processes is crucial for improved water resource management. Our study assessed wildfire severity impacts on hydrology using a modified calibration method for the Soil and Water Assessment Tool (SWAT) model. Calibration incorporated evapotranspiration and leaf area index to represent vegetation loss and hydrologic impacts. We also integrated a wildfire module to simulate fire effects on soil and vegetation parameters. This improved modeling approach effectively captured post-fire hydrologic behavior, especially increased high streamflows and reduced evapotranspiration, with greater changes linked to higher burn severity. These findings emphasize the importance of considering fire severity in hydrologic modeling, aiding proactive management and mitigation strategies to protect water supply and enhance ecosystem resilience in wildfire-prone regions.

1. Introduction

Larger, more severe wildfires have increased in the Pacific Northwest (PNW) in recent decades, raising concerns about effects on hydrologic processes, streamflow, water quality, aquatic ecosystems, and drinking water treatment (Bladon et al., 2014; Robinne et al., 2020). Wildfires can have significant and long-lasting impacts on many hydrological processes (Long and Chang, 2022; Robinne et al., 2020). For example, loss of forest canopy and ground cover can lead to decreased interception losses and greater net precipitation (Ma et al., 2020; Williams et al., 2019). Despite this increase in net precipitation, numerous studies have observed reductions in evapotranspiration (ET) at stand or watershed scales due to vegetation loss (Collar et al., 2021; Ma et al., 2020; Niemeyer et al., 2020; Poon and Kinoshita, 2018). In addition to the ET reduction, the combined effects of additional water reaching the soil surface and altered runoff pathways often lead to changes in peak flows, and annual water yields, which can persist for many years after a wildfire (Hallema et al., 2017; Holden et al., 2012; Stoof et al., 2012). Furthermore, wildfires modify soil physical properties, such as surface sealing, ash deposition, and development of water-repellent layers, leading to altered infiltration, surface runoff, hillslope runoff, and erosion processes (Ebel et al., 2012; Ebel and Moody, 2020; Moody et al., 2015). These soil alterations also affect soil moisture dynamics by altering soil physical properties (González-Pelayo et al., 2024; Stevens et al., 2020), potentially influencing vegetation recovery and plant regrowth after wildfire disturbances (Yang et al., 2022).

Fire severity, which refers to the extent of vegetation impacts, and soil alteration caused by a wildfire, is a critical determinant of post-fire hydrological changes. For instance, Kang et al. (2024) studied the effects of the 2020 Labor Day Fires in the Western Cascades of Oregon on runoff and ET in several catchments and found that decreases in ET and increases in runoff were strongly correlated with burn severity and burned area. Additionally, a study in the Pacific Northwest region found that watersheds burned at medium to high severity experienced post-fire peak flow increases of 21–34 %, while low severity areas tended to have minimal (~2 %) impacts on peak flows (Li et al., 2023). However, the relationship between fire severity and hydrological responses is complex and influenced by various factors, leading to substantial uncertainty and variability in outcomes (Saxe et al., 2018; Spencer and Winkler, 2024). In addition, empirical studies are often constrained

* Corresponding author. Department of Civil and Environmental Engineering, Washington State University, Pullman, WA, USA.
E-mail address: hyunwoo.kang1@wsu.edu (H. Kang).

https://doi.org/10.1016/j.envsoft.2026.106896
Received 22 April 2025; Received in revised form 24 December 2025; Accepted 24 January 2026
Available online 24 January 2026

spatially and temporally, which limits the transferability of knowledge and our ability to make accurate predictions (Emmerton et al., 2020; Wu et al., 2021).

Hydrologic models are often used as an effective tool for examining wildfire impacts on hydrology under multiple post-fire scenarios and scales because they incorporate complex hydrologic processes (Ebel et al., 2023; Kiesel et al., 2013; Loiselle et al., 2020; Wampler et al., 2023). Many hydrologic models have been adapted and used to evaluate hydrologic response to wildfires, with different models suited to various spatial and temporal scales (Ebel et al., 2023). For example, the Regional Hydro-Ecologic Simulation System (RHESSys; Tague and Band, 2004) model was used to assess catchment-scale effects from wildfire on vegetation carbon cycle (Bart et al., 2020), and impacts of climate change on wildfire regimes (Hanan et al., 2021). Similarly, the Water Erosion Prediction Project (WEPP; Elliot, 2004) is a process-based hydrology and erosion model used to simulate wildfire effects on water quantity and quality (Dobre et al., 2022). These examples illustrate how different models operate at varying spatial scales, with each model offering unique strengths in capturing specific aspects of fire-hydrology interactions.

The Soil and Water Assessment Tool (SWAT; Arnold et al., 1998; Neitsch et al., 2011) model is a semi-distributed, continuous, and process-based model, which has increasingly been used in recent years to evaluate wildfire impacts on hydrology at a river basin scales (Basso et al., 2020; Loiselle et al., 2020; Wampler et al., 2023). Compared to other hydrologic models used to evaluate wildfire effects on hydrology, SWAT has been applied to relatively large-scale watersheds and has reduced process complexity compared to other models (Ebel et al., 2023). Originally developed for use primarily in agricultural systems, SWAT has been modified to improve hydrological simulations in forested ecosystems by updating plant growth, forest dynamics, and nutrient cycling (Lai et al., 2020; Yang and Zhang, 2016; Zhang et al., 2020). More recently, Haas et al. (2022a, 2022b) proposed a new calibration method to improve simulation of forest processes by reparameterization of forest vegetation, including the calibration of ET, biomass, and leaf area index (LAI), leading to improved water balance simulations in forested watersheds. These modifications have improved the suitability of SWAT for modeling wildfire-induced changes in hydrology across large watersheds while maintaining computational efficiency.

In recent decades, there has been a substantial increase in the amount and type of hydrologic data available from satellite and remote sensing products, including data on precipitation, soil moisture, groundwater levels, snow cover, and evapotranspiration, which have improved our ability to understand the hydrologic cycle. Among the datasets representing ET, NASA's Moderate Resolution Imaging Spectrometer (MODIS) dataset has been widely used for calibration with the SWAT model in the US (Dangol et al., 2023; Koltsida and Kallioras, 2022). Multiple studies have used MODIS ET data to calibrate SWAT and achieve improved watershed model predictions (Parajuli et al., 2018; Tobin and Bennett, 2017), demonstrating the value of using remote sensing-based ET data. However, previous wildfire studies using the SWAT model have not incorporated ET calibration specifically in forested watersheds. While other studies have used SWAT to examine wildfire impacts on streamflow and peak flow (Wampler et al., 2023), and improved it for use in forested watersheds by integrating ET and LAI calibration (Haas et al., 2022b), no study has combined both of these calibrations in the context of wildfire-affected forested watersheds. Therefore, SWAT has been underutilized for addressing post-fire hydrological dynamics and fire severity effects. Recently, the SWAT + model (Bieger et al., 2017) has been developed as the latest generation of the SWAT family, providing enhanced spatial flexibility and improved representation of land management operations, including the capability to incorporate fire operations within the management module. Our study used the SWAT 2012 version, which remains widely applied and validated for wildfire-related hydrologic simulations (Wampler et al., 2023), while the calibration framework and wildfire parameterization presented here are consistent with the structural concepts introduced in SWAT+.

In our study, we built on these recently developed methods for improved calibration of SWAT simulation of forest and wildfire dynamics. We implemented additional wildfire calibration steps to further improve the wildfire module, and we evaluated the modified SWAT simulations of wildfire-driven hydrologic change. By addressing this gap, we aimed to advance the use of SWAT for wildfire impact analysis in forested watersheds. Specifically, we evaluated impacts of large, high severity wildfires on hydrological fluxes in two basins in the Western Cascades of Oregon, USA that burned during the 2020 Labor Day Fires. During these events, five large wildfires (Archie Creek, Beachie Creek, Holiday Farm, Lionshead, and Riverside) burned more than 343,900 ha and destroyed more than 4000 homes (Oregon Department of Forestry, 2022). Unusually dry conditions and strong east winds helped fuel the fires and caused them to spread quickly and burn severely (Abatzoglou et al., 2021). These events highlighted critical knowledge gaps regarding how wildfire severity influences post-fire changes in ET, runoff, and streamflow, and overall water balance. The specific objectives of our study were to:

a. Develop and apply a modified calibration technique and wildfire module to the SWAT model to simulate hydrological fluxes in forested watersheds affected by wildfire;
b. Use empirical hydrological data to evaluate the pre- and post-fire performance of simulations from the default and modified SWAT calibration techniques;
c. Assess post-fire hydrological responses, including changes in ET, runoff, streamflow, and annual water balance; and
d. Evaluate the role of fire severity in mediating post-fire hydrological responses.

2. Methods

2.1. Study area

For our study, we selected two large sub-basins in the Cascade Range in Oregon, USA, which are tributaries of the Willamette River Basin (Fig. 1). The McKenzie River sub-basin provides drinking water to about 200,000 people in the Eugene area in Oregon (Kraus et al., 2010), and the North Santiam River sub-basin supplies water to approximately 200,000 residents in the Salem area in Oregon. The watersheds are located within a Mediterranean climate with dry, warm summers and cool, wet winters (Snyder et al., 2002). Average annual precipitation of the two watersheds is 2204 mm, but varies from 1124 mm to 3164 mm due to orographic effects (PRISM Climate Group, 2022). Elevation across the sub-basins ranges from 139 m to 3194 m (Fig. 1b). In the lower elevation areas (<300 m), annual 30-year normal temperatures range from mean daily minimums of 0.2–1.4 °C in the winter to mean daily maximums of 24.8–28.3 °C in the summer. In the high elevation areas (>1700 m) temperatures range from mean daily minimums of −8.0 to −1.4 °C in the winter to mean daily maximums of 19.4–26.0 °C in the summer (PRISM Climate Group, 2022). Both watersheds are primarily dominated by evergreen forests (~80 %) of Douglas-fir (*Pseudotsuga menziesii*), Pacific silver fir (*Abies amabilis*), and Western hemlock (*Tsuga heterophylla)* (Table 1). The dominant soil textures include Silty Clay Loam, Clay Loam, and Cobbly Loam (NRCS, 2025). Geologically, the watersheds are situated on volcanic formations of the Cascade Range, composed mainly of basaltic and andesitic lava flows, pyroclastic deposits, and glacial sediments (Tague and Grant, 2004). These characteristics influence groundwater–surface water interactions, with extensive spring-fed systems in the High Cascade terrain sustaining streamflow during the dry season (Jefferson et al., 2006).

In September 2020, three wildfires occurred through the McKenzie and North Santiam watersheds, burning a total area of 146,580 ha inside

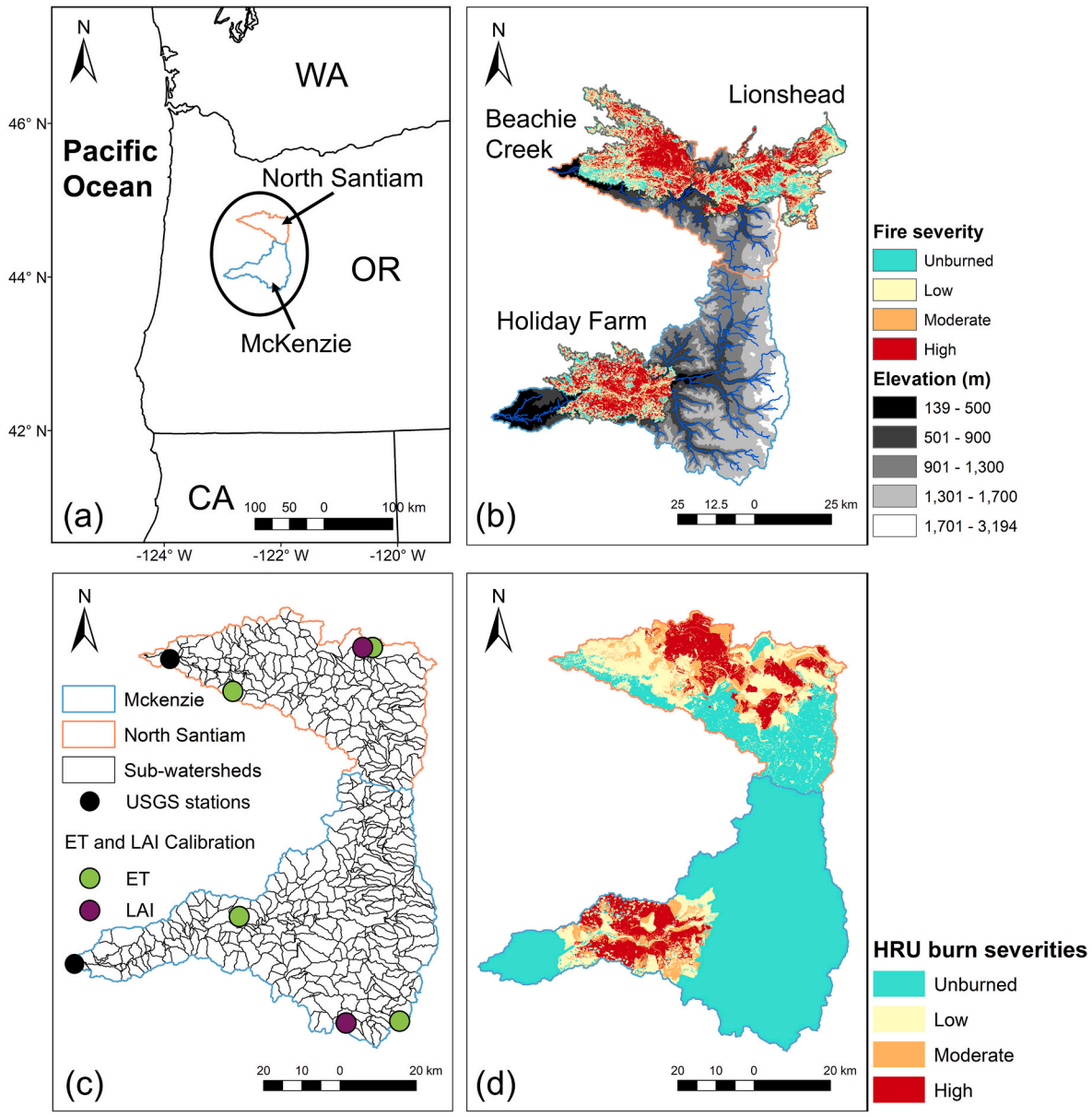

Fig. 1. (a) Map showing the location of our study watershed (black circle) in the western United States. Blue and red lines highlight the McKenzie and North Santiam watersheds, respectively. (b) Map of the study watersheds and three wildfires burned in 2020 (from north to south: Beachie Creek, Lionshead, and Holiday Farm). In the burned areas, aqua, light yellow, orange, and red areas indicate the unburned, low, moderate, and high burned severities. (c) Sub-watersheds and calibration locations. Black lines represent the boundaries of the sub-watersheds, black circles indicate the USGS gauging stations for streamflow calibrations, and the green and blue circles represent the locations of ET and LAI calibrations (USGS: United States Geological Survey, ET: Evapotranspiration, LAI: Leaf area index). (For interpretation of the references to colour in this figure legend, the reader is referred to the Web version of this article.)

Table 1
General characteristics of the McKenzie and North Santiam watersheds.

	McKenzie	North Santiam
Watershed Area (ha)	175,141	295,777
Land uses (Natural Resources Conservation Service, 2025; Dewitz and USGS, 2021)	Evergreen Forest (84 %), Shrub (7 %), Barren Land (3 %),Pasture/Hay (1 %)	Evergreen Forest (84 %), Shrub (8 %), Pasture/Hay (2 %)
Soils Textures (NRCS, 2025)	Silty Clay Loam, Clay Loam and Cobbly Loam	Silty Clay Loam, Clay Loam and Cobbly Loam
Elevation (m)	Mean: 1045 Min: 139 Max: 3149	Mean: 983 Min: 146 Max: 3193

the watersheds perimeters (Fig. 1b). In the McKenzie River sub-basin, the Holiday Farm Fire affected approximately 18 % of the sub-basin area (56,394 ha). Within the watershed, the wildfire burned at relatively high severity with 13.2 % unburned, 14.5 % low, 35.3 % moderate, and 37.1 % high severity (Table 2). The Beachie Creek and Lionshead Fires burned about 77 % of the North Santiam watershed (90,186 ha). The Beachie Creek Fire burned 44.2 % of the sub-basin area (51,738 ha) with 16.4 % unburned, 18.4 % low, 30.3 % moderate, and 34.9 % high severity. The Lionshead Fire burned 38.8 % of the sub-basin area (38,448 ha) with 19.9 % unburned, 19.6 % low, 28.6 % moderate, and 31.9 % high severity. Given the differences in both the area and magnitude of these wildfires across the two sub-basins, we expected the magnitude and range of hydrologic responses to differ between the study catchments, providing a useful comparison.

Table 2
Information of the three wildfires that burned in the North Santiam and McKenzie Basins in 2020. Burn severity classes were categorized based on the difference Normalized Burn Ratio (dNBR) values proposed by Key and Benson (2006). The dNBR data is from the monitoring trends in burn severity (MTBS, 2024) website (https://mtbs.gov/).

Wildfires	Watersheds	Total area burned (ha)	Burned area in watershed (ha)	Burn severity within basin (%)			
				Unburned (dNBR≪ 100)	Low (dNBR ≥ 100 and < 270)	Moderate (dNBR ≥ 270 and < 660)	High (dNBR ≥ 660)
Holiday Farm	McKenzie	70,169	56,394	13.2	14.5	35.3	37.1
Beachie Creek	North Santiam	78,333	51,738	16.4	18.4	30.3	34.9
Lionshead	North Santiam	82,794	38,448	19.9	19.6	28.6	31.9

2.2. SWAT model background and calibration

SWAT is a semi-distributed, continuous, and process-based hydrologic model developed to simulate the long-term effects of climate and land use management on hydrology, sediment transport, and water quality in watersheds (Arnold et al., 1998; Neitsch et al., 2011). In our study, we used the SWAT 2012 model (rev. 664) with the ArcSWAT 2012.10.5 interface. Watersheds were delineated into sub-watersheds using digital elevation models. Each sub-watershed was further divided into hydrologic response units (HRUs), which represent unique combinations of land use, soil type, and slope class within each subbasin. The use of HRUs enabled us to account for spatial heterogeneity in land cover, soil, and topography within the model.

We used a 30 m digital elevation model (DEM) from the National Hydrography Dataset (NHD) (U.S. Geological Survey, 2022) for watershed configuration and topographic parameter estimation. Land use and soil inputs were based on 2019 National Land Cover Database (NLCD) data (Dewitz and USGS, 2021) and STATSGO2 soils data (NRCS, 2025). The Blue River and Cougar Reservoirs in the McKenzie River sub-basin, along with the Detroit Reservoir in the North Santiam sub-basin, were included in the model simulation by configuring reservoir surface areas and volumes for both emergency and principal spillways. Additionally, monthly reservoir outflow data were incorporated to account for flow alterations caused by the reservoirs (U.S. Army Corps of Engineers, 2025). For meteorological inputs, we used Daymet precipitation and temperature data at a 1-km resolution (Thornton et al., 2022). The watershed delineation resulted in 313 sub-watersheds for the McKenzie and 203 for the North Santiam sub-basin (Fig. 1c), with the watershed outlets set at the approximate drinking water intake locations for Eugene (McKenzie) and Salem (North Santiam). Sub-watersheds were then divided into HRUs, resulting in 2048 HRUs for the McKenzie and 1248 HRUs for the North Santiam to represent the pre-fire conditions. To reduce computational load, we applied 10 % threshold values for land use, soil, and slope, dissolving HRUs that fell below these thresholds into existing land use, soil, and slope categories (Her et al., 2015).

Calibration and validation are essential to ensuring the reliability of hydrological processes under varying conditions. Daily streamflow was calibrated using the SWAT calibration and uncertainty assessment tool SWAT-CUP (Abbaspour, 2014) with the SUFI-2 method. The model was run on a daily time step, with a 3-year warm-up period. Calibration was performed for discharge from January 2011 to August 2020 (pre-wildfire period), using streamflow data from US Geological Survey (USGS) gauge stations (McKenzie: USGS 14164900, North Santiam: USGS 14183000). Validation was conducted over a separate period from 2001 to 2010 at the same stations. This design ensured that model parameters were calibrated to reflect hydrologic conditions immediately before the wildfire, allowing for continuity with the post-fire simulation and improved the ability of the model to detect wildfire-driven changes.

To improve SWAT model simulations in forested environments and to account for wildfire effects, we compared two calibration processes: (1) the default simulation (hereafter referred to as the “default” model), which is parameterized for non-forest ecosystems and is calibrated using only streamflow data, and (2) a modified simulation (hereafter referred to as the “modified” model), which included calibration of streamflow, ET, and LAI, designed to more accurately reflect interactions between forest processes and hydrological computations within SWAT. Haas et al. (2022a, b) proposed this approach to improve representation of forest hydrology of the SWAT model by incorporating additional vegetation dynamics, particularly LAI and ET, into the calibration process. For example, LAI is used to calculate plant biomass and evapotranspiration partitioning (e.g., canopy evaporation and transpiration), which differs greatly between forested and non-forest environments and is critical in capturing disturbance effects like those caused by wildfire. For ET and LAI calibrations, we used 500 m resolution MOD15A2H (Myneni et al., 2015) and MOD16A2 (Running et al., 2017) datasets to derive LAI and ET time series data at 8-day intervals for two sub-basins primarily composed of evergreen forest (>80 %) (Hass et al., 2022a, b).

Calibration was carried out using the Nash–Sutcliffe Efficiency (NSE; Nash and Sutcliffe, 1970) as the primary objective function, as it effectively measures the correspondence between observed and simulated daily streamflow (Moriasi et al., 2015). The initial parameter ranges were established using the default limits provided in the SWAT-CUP interface. The number of calibration iterations differed by basin and calibration types because the parameter ranges were progressively narrowed until all calibration variables reached satisfactory ranges. For the McKenzie River sub-basin, the default simulation required three iterations, whereas the modified calibration required 38 iterations. For the North Santiam sub-basin, the default simulation required two iterations, and the modified calibration required 15 iterations. Each iteration consisted of 1000 simulations, with parameter ranges adjusted based on the best-performing parameter sets and constrained by plausible values documented in previous SWAT studies (Abbaspour, 2014; Abbaspour et al., 2015; Haas et al., 2022a, 2022b; Narsimlu et al., 2015; White et al., 2018; Lee et al., 2024; Devkota et al., 2024). Model validation followed a split-sample approach, applying the single best parameter set from the calibration to the independent validation period. This approach ensured that the model was evaluated under different hydrologic conditions without recalibration. For streamflow, model performance during calibration was first evaluated against the “Good” performance (NSE >0.70) for daily simulations (Moriasi et al., 2015), confirming that the model achieved acceptable predictive accuracy.

Parameters used in the default and modified models are listed in Table 3, and additional vegetation-related parameters applied in the modified model are presented in Table 4. To account for spatial heterogeneity, separate parameter sets were calibrated for the upstream and downstream sub-basins, while basin-level and plant parameters were applied uniformly across the watershed. For the McKenzie watershed, the upstream and downstream areas were divided at the confluence of the Blue River and the South Fork McKenzie River, whereas in the North Santiam watershed, the division was defined by the location of Detroit Dam, which integrates inflows from multiple upstream tributaries. This approach was supported by the SWAT-CUP framework,

Table 3
Summary of SWAT calibrated parameters for both default and modified models.

Parameter	Description	Range	
		Min	Max
r_ CN2.mgt	SCS runoff curve number	−0.3	0.3
v_ALPHA_BF.gw	Baseflow alpha factor (days)	0.2	0.6
v_GW_DELAY.gw	Groundwater delay (days)	100	400
v_GWQMN.gw	Threshold depth of water in the shallow aquifer required for return flow to occur (mm)	0	1000
v_ESCO.hru	Soil evaporation compensation factor	0.01	1
v_EPCO.hru	Plant uptake compensation factor	0.01	1
v_SOL_AWC.sol	Available water capacity of the soil layer (mm H_2O/mm soil)	0	1
r_ SOL_K.sol	Saturated hydraulic conductivity (mm/hr)	−0.3	0.3
r_ SOL_BD.sol	Moist bulk density (g/cm^3)	−0.5	0.3
v_GW_REVAP.gw	Groundwater "revap" coefficient	0.02	0.2
v_SURLAG.hru	Surface runoff lag time (days)	1	24
v_OV_N.hru	Manning's "n" value for overland flow	0.01	1
v_TIMP.bsn	Snow pack temperature lag factor	0	1
v_SFTMP.bsn	Snowfall temperature (°C)	−10	10
v_SMTMP.bsn	Snow melt base temperature (°C)	−10	10
v_SMFMX.bsn	Maximum melt rate for snow during year (mm H_2O/°C-day)	0	5
v_SMFMN.bsn	Minimum melt rate for snow during the year (mm H_2O/°C-day)	0	5
v_CANMX.hru	Maximum canopy storage (mm H_2O)	0	100
r_SLSUBBSN.hru	Average slope length (m)	−0.2	0.2
r_HRU_SLP.hru	Average slope steepness (m/m)	−0.3	0.3
v_CH_K2.rte	Effective hydraulic conductivity in main channel alluvium	0.01	500
v_CH_N2.rte	Manning's "n" value for the main channel	0.001	1
r_ SOL_Z.sol	Depth from soil surface to bottom of layer	−0.5	0.5
v_LAI_INIT.mgt	Initial leaf area index (m^2/m^2)	0	3
v_PHU_PLT.mgt	Total number of heat unit	1000	3000

Note: v_, denotes the default parameter is replaced by a given value; r_, means the existing parameter value is multiplied by (1 + a given value).

which allows spatially differentiated parameterization. In the modified (multi-variable) calibration, we assigned weights of 0.3 to streamflow, 0.2 to LAI, and 0.25 to ET in each of the two sub-watersheds, resulting in a total weight of 1. This weighting scheme balanced hydrologic and vegetation components and ensured that no single variable disproportionately influenced the calibration outcome.

Given that evergreen forest covers more than 80 percent of both study basins, vegetation dynamics such as ET and LAI were expected to be relatively homogeneous across the study area. Therefore, calibration with MODIS-based observations in representative areas was considered to capture the dominant basin-wide vegetation signals. This approach was supported by Haas et al. (2022a, b), who reported that sub-watershed calibration using representative forested areas can effectively capture vegetation process in forested watersheds. In both the McKenzie and North Santiam watersheds, we selected two forested sub-watersheds for ET and one HRU for LAI calibration. For ET calibration, the selected sub-watersheds were 304 (1404 ha) and 125 (1349 ha) in the McKenzie basin, and 37 (816 ha) and 121 (1840 ha) in the North Santiam basin, representing upstream and downstream locations (Fig. 1c). For LAI calibration, we selected one evergreen forest HRU in each basin, and they are HRU 2037 in McKenzie (323 ha) and HRU 221 in North Santiam (231 ha). This targeted calibration strategy also helped reduce model complexity and minimize parameter equifinality compared to full-watershed calibration that selected multiple sub-watersheds to cover the entire watershed, which involves a larger number of parameters that can complicate model optimization (Abbaspour et al., 2015; Yang et al., 2008).

Table 4
Summary of SWAT calibrated parameters for the modified model (user-defined forest parameters which impact watershed hydrological processes) (Haas et al., 2022a; 2022b).

Parameter	Description	Range	
		Min	Max
v_GSI in plant.dat	Max stomatal conductance (m*s^{-1})	0.001	0.1
v_CHTMX in plant.dat	Max canopy height (m)	0.1	20
v_RDMX in plant.dat	Max root depth (m)	0	3
v_VPDFR in plant.dat	Vapor pressure deficit corresponding to the fraction maximum stomatal conductance (kPa)	0.7	3.7
v_BIO_E in plant.dat	Biomass/Energy Ratio ((kg/ha)/(MJ/m^2))	0.1	50
v_BLAI in plant.dat	Max leaf area index	0.5	5
v_T_OPT in plant.dat	Optimal temperature (temp) for plant growth (°C)	10	30
v_T_BASE in plant.dat	Min temp plant growth (°C)	0	4
v_BIO_LEAF in plant.dat	Fraction of tree biomass converted to residue during dormancy	0	1
v_EXT_COEF in plant.dat	Light extinction coefficient	0.1	2
v_BMX_TREES in plant.dat	Maximum biomass for a forest (metric tons/ha)	100	1000
v_ALAI_MIN in plant.dat	Minimum leaf area index for plant during dormant period (m^2/m^2)	0	1
v_DLAI in plant.dat	Fraction of growing season when leaf area starts declining	0.15	1

Note: v_, denotes the default parameter is replaced by a given value.

After calibration, model evaluation of the two simulations was conducted using both statistical and graphical approaches. Streamflow performance was evaluated at point locations (USGS gauge stations) using NSE, coefficient of determination (R^2), root mean square error (RMSE), and percent bias (PBIAS). ET and LAI simulations were compared with MODIS observations (Myneni et al., 2015; Running et al., 2017) at the catchment level using the same set of statistical metrics and graphical approaches. Water-balance partitioning was also compared between the default and modified models using long-term averages of ET, baseflow, lateral flow, and surface runoff, summarized as percentage contributions to total precipitation.

2.3. *Wildfire module and evaluation*

In addition to the modified calibration technique described above, we incorporated the SWAT wildfire module developed by Wampler et al. (2023), which modified multiple soil and vegetation parameters based on burn severities in the SWAT model to represent the effects of wildfires. In SWAT simulations, we set the fire date to September 7, 2020, which marked the beginning of the Holiday Farm fire and the rapid expansion of the other two wildfires. To assign fire severities to each HRU, we employed the "Zonal Statistics as Table" tool in ArcMap to compute the mean dNBR (differenced normalized burn ratio; Key and Benson, 2006) values for each HRU. The burn severity and burned perimeters data were provided by the Monitoring Trends in Burn Severity ("MTBS," 2024), and the averaged burn severity was used to classify low, moderate, and high burn severity categories. We selected dNBR values at <100 for unburned, <270 for low burn severity, <660 for moderate burn severity, and ≥ 660 for high burn severity (Key and Benson, 2006), and dNBR-based classification is widely applied to assess fire-induced changes in vegetation and soil properties, as it captures the degree of organic matter consumption and canopy alteration (Keeley, 2009).

The wildfire module accounts for the impacts of wildfires by adjusting several critical model parameters. These adjustments included

modifications to available water capacity, bulk density, soil and plant evaporative compensation factors, curve number, Manning's n for overland flow, and land use. The parameter modifications were initiated from the date of the wildfire event, reflecting the immediate and long-term effects of the fire on the landscape. Using the model with adjusted parameters, we ran the model for three years following the fires, as data were available only for this period, and compared the results with baseline simulations (SWAT-normal). To assess the accuracy of the wildfire simulations (SWAT-fire), we compared simulated streamflow and ET of the normal and wildfire simulations with observed streamflow data and remotely sensed ET for pre- and post-fire periods. We ran both the SWAT-normal and SWAT-fire simulations using the modified calibration that incorporated streamflow, ET, and LAI. Wildfire-related parameter modifications were applied only to the SWAT-fire simulation to represent the effects of wildfire. Detailed descriptions of these parameter changes are available from Wampler et al. (2023) and summarized in Table 5.

After applying the wildfire module, streamflow performance was evaluated under both overall and high-flow conditions (>90th percentile of daily discharge) to assess model behavior after wildfires. ET and runoff responses to wildfire severity were further analyzed at the sub-watershed scale. Box-and-whisker plots were used to summarize spatial variability across burn-severity classes (unburned, low, moderate, and high), while scatter plots with dNBR were used to quantify the relationships between burn severity and percent changes in ET and runoff. Water-balance partitioning was also evaluated by comparing the relative contributions of ET, surface runoff, lateral flow, and baseflow between the SWAT-normal and SWAT-fire simulations to assess wildfire-induced changes in hydrologic processes.

3. Results

3.1. Base model calibration for forested systems

The default and modified calibration procedures produced similar streamflow simulations in both watersheds (Table 6). Also, the final calibrated parameter values for the default and modified models are provided in the Supplementary material (Table S1–S3). In the McKenzie watershed, the modified model slightly outperformed the default during the calibration period (NSE = 0.88 vs. 0.87; R^2 = 0.90 vs. 0.88), while validation results were similar. In the North Santiam watershed, both models showed modest differences, with NSE ranging from 0.67 to 0.74 and R^2 from 0.70 to 0.78 across periods. Full performance metrics are provided in Table 6. To complement these statistical results, the observed and simulated hydrographs for both watersheds are presented in the Supplementary Materials (Fig. S1–S2). These figures present that both the default and modified simulations reproduced the seasonal variability of streamflow well, and the NSE values for both watersheds indicate Good (NSE >0.70) to Very Good (NSE >0.85) model performance (Moriasi et al., 2015).

The SWAT model captured general seasonal variation in ET (NSE >0) across all sites using both the default and modified models (Fig. 2). However, the default model tended to underestimate ET in summer and overestimate it in winter, while the modified calibration reduced these biases. For instance, in sub-watershed 125 (McKenzie) NSE improved from 0.18 (default) to 0.48 (modified), while in 121 (North Santiam) the NSE improved from 0.38 (default) to 0.60 (modified). These improvements were also reflected in improved R^2 and PBIAS values (Table 6), indicating better seasonal agreement with MODIS ET.

The modified LAI parameterization substantially improved LAI simulations compared to the default model, which was not calibrated for forested systems (Fig. 3). In both HRU 2037 (McKenzie) and HRU 221 (North Santiam), the default model failed to capture seasonal dynamics (NSE <0), while the modified model reproduced typical seasonal patterns, including the spring increase and late-summer decline in streamflow, with NSE improving to 0.66 and 0.45, respectively in the two sub-basins. These results demonstrated that forest-specific parameterization enhanced the model's ability to simulate vegetation dynamics in fire-prone watersheds (Table 6). In addition, we compared SWAT-simulated monthly ET and LAI values against MODIS observations for the entire McKenzie and North Santiam watersheds using the calibrated parameters to evaluate whether sub-watershed-based calibration effectively captured basin-wide vegetation dynamics. As shown in Figs. S3 and S4 in the Supplementary Material, SWAT successfully reproduced seasonal patterns and magnitudes of ET, with NSE values of 0.78 for McKenzie and 0.86 for North Santiam during the calibration period (2011–August 2020) (Fig. S3). Similarly, SWAT captured seasonal LAI dynamics, with NSE values of 0.31 for McKenzie and 0.52 for North Santiam (Fig. S4). These results are consistent with those obtained in the representative sub-watersheds used for calibration (Figs. 2 and 3), indicating that the selected areas adequately represented vegetation behavior across the basins.

3.2. Comparison of water balance partitioning

In addition to the improvements in ET and LAI estimations, the modified parameterization led to clear differences in water balance partitioning. Both models indicated that ET and lateral flow was the dominant component of the water budget for both the McKenzie and North Santiam River sub-basins during the calibration and validation period from 2001 to September 2020. For the McKenzie River sub-basin, ET and lateral flow accounted for 35.6 % and 29.4 % of the water budget in the default model, while baseflow accounted for 26.7 %, and surface runoff accounted for 8.4 % (Fig. 4a). Under the modified model, ET and lateral flow increased to 37.8 % and 35.8 % while baseflow decreased slightly to 23.1 % and surface runoff decreased more substantially to 3.3 %. Considering only total runoff, the contributions of surface runoff were 17.5 % from the default model and 10.1 % from the modified model.

Similar patterns were observed in the North Santiam River sub-basin. In the modified model, baseflow increased from 12.7 % to 21.2 %, while surface runoff decreased from 12.0 % to 7.1 % (Fig. 4b). Lateral flow remained the largest runoff component, accounting for about 42–43 % in both models, indicating that subsurface flow dominates hydrologic responses in this basin. ET also decreased slightly from 31.5 % to 29.6 %, but the seasonal pattern of ET was improved under the modified model (Fig. 2b), likely reflecting the influence of revised water-balance partitioning. These results from both sub-basins highlight the shift toward stronger subsurface contributions and reduced surface runoff under the modified calibration, consistent with the hydrologic characteristics of the western Cascade watersheds (McGuire and McDonnell, 2010).

3.3. Wildfire simulation

3.3.1. Comparison of simulated runoff and ET before and after wildfire for SWAT-normal and SWAT-fire simulations

Simulation results from SWAT-fire showed slight increases in streamflow (3.1 % in the McKenzie and 4.8 % in the North Santiam) compared to SWAT-normal, especially during the wet seasons (October

Table 5
Summary of parameters modified in the wildfire module (Wampler et al., 2023).

Parameter	Replacement type	Change based on fire severity		
		Low	Moderate	High
SOL_AWC	relative	−25 %	−70 %	−90 %
SOL_BD	relative	1 %	9 %	13 %
ESCO	replace	0.5	0.8	1
EPCO	replace	0.5	0.2	0.01
CN2	additive	10	20	30
OV_N	replace	0.8	0.4	0.011
Land Use	replace	FRSE	RNGE	BARR

Table 6
Results of calibration and validation for the default and modified model.

Watersheds	Calibration/ Validation	Evaluation criteria	Default model				Modified model			
			Streamflow	ET subbasin 125	ET subbasin 304	LAI HRU 2037	Streamflow	ET subbasin 125	ET subbasin 304	LAI HRU 2037
McKenzie	Calibration (2011–Aug 2020)	NSE	0.87	0.18	0.44	−0.85	0.89	0.49	0.47	0.66
		R^2	0.88	0.34	0.69	0.02	0.90	0.56	0.79	0.73
		RMSE	34.51	1.30	0.72	1.07	33.65	1.02	0.70	0.46
		PBIAS (%)	5.00	21.41	−20.30	−19.84	4.16	13.01	−20.77	4.42
	Validation (2001–2010)	NSE	0.78	0.13	0.22	−0.57	0.73	0.45	0.23	0.61
		R^2	0.82	0.28	0.66	0.00	0.82	0.50	0.75	0.69
		RMSE	41.62	1.28	0.76	1.09	46.88	1.01	0.76	0.54
		PBIAS	10.74	14.21	−26.23	12.94	9.73	7.59	−26.84	1.34
North Santiam	Calibration (2011–Aug 2020)	NSE	0.74	0.41	0.38	−0.74	0.71	0.45	0.60	0.45
		R^2	0.78	0.57	0.47	0.21	0.76	0.53	0.62	0.69
		RMSE	38.89	0.95	1.02	1.69	40.86	0.92	0.82	0.95
		PBIAS	13.07	−8.07	6.49	43.09	11.14	2.70	5.94	13.21
	Validation (2001–2010)	NSE	0.67	0.10	0.41	−0.47	0.69	0.41	0.61	0.66
		R^2	0.70	0.51	0.49	0.09	0.72	0.51	0.62	0.71
		RMSE	43.37	1.07	0.96	1.87	41.89	0.87	0.78	0.90
		PBIAS	15.32	−15.73	0.06	38.17	11.77	−2.83	5.65	11.29

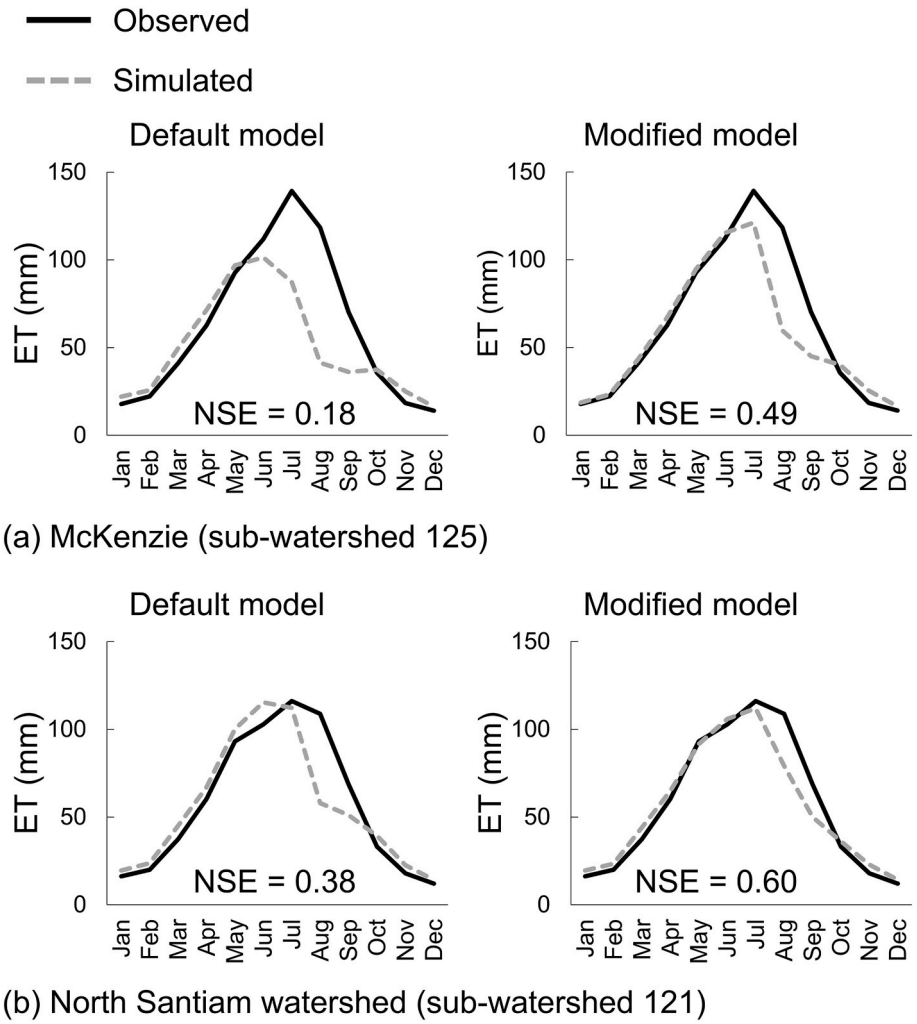

Fig. 2. Comparisons of monthly average ET from the default and improved calibration technique. The monthly average was determined by averaging the daily data, not the sum of daily data. Black lines indicate the remote sensing observations (MODIS: Moderate Resolution Imaging Spectrometer), and gray and dashed lines represent the ET estimates from SWAT. (a) Results of the McKenzie watershed (sub-watershed 125). (b) Results of the North Santiam watershed (sub-watershed 121).

to March) (Fig. 5). Overall performance of streamflow simulations were similar between SWAT-fire and SWAT-normal during the post-fire

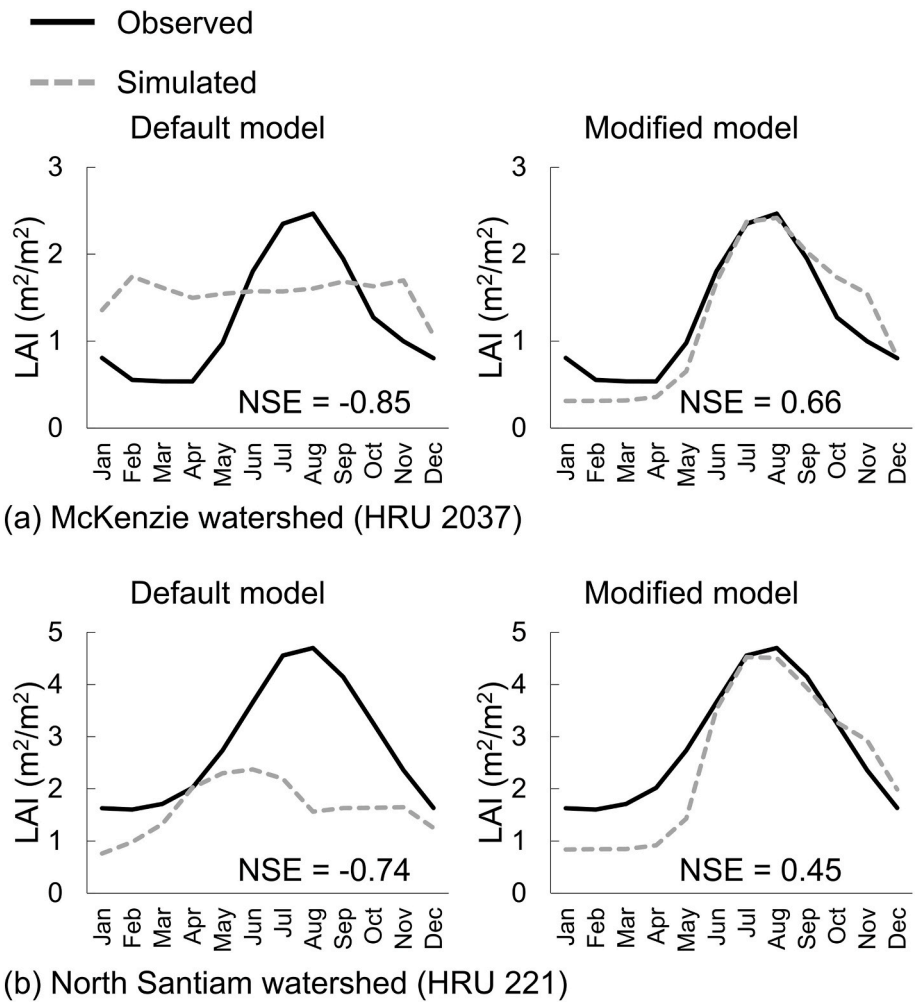

Fig. 3. Comparisons of monthly average LAI from the default and improved calibration technique. Black lines indicate the remote sensing observations (MODIS), and gray and dashed lines represent the LAI estimates from SWAT. (a) Results of the McKenzie watershed (HRU, 2037). (b) Results of the North Santiam watershed (HRU 221).

period. In the McKenzie and North Santiam watersheds, both simulations achieved identical NSE values (0.88 in McKenzie and 0.66 in North Santiam), although the PBIAS was slightly more accurate for the SWAT-fire simulation compared to the normal simulation (Fig. 5). However, the SWAT-fire simulation demonstrated superior performance in simulating high flow conditions (>90th percentile) in both watersheds. In the McKenzie watershed, the NSE for high flow was 0.85 for the SWAT-fire simulation, compared to 0.53 for the SWAT-normal simulation (Fig. 5b). Likewise, in the North Santiam watershed, the SWAT-fire simulation generated better simulation (NSE = 0.03), outperforming the SWAT-normal simulation (NSE = −0.65) (Fig. 5d).

Increased streamflow was primarily driven by enhanced surface runoff in burned sub-watersheds. In the McKenzie sub-basin, runoff increases were consistently higher in areas with greater burn severity and were most pronounced in 2022, the wettest post-fire year (1965 mm of precipitation), compared to 2021 (1710 mm) and 2023 (1636 mm) (Fig. 6a–c). Linear regression analysis confirmed a strong positive relationship between runoff change and burn severity, with R^2 values ranging from 0.68 to 0.81 (Fig. 6d–f). A similar pattern was observed in the North Santiam watershed, where runoff increases also scaled with burn severity and peaked in 2022. The strength of correlation between runoff changes and dNBR ranged from 0.53 to 0.79, reinforcing the consistent influence of burn severity across years and watersheds (Fig. 7a–f).

The severe wildfires in 2020 led to substantial reductions in ET during the post-fire period (October 2020 to September 2023). Relative to the SWAT-normal simulation, there was an overall decrease in ET in the SWAT-fire simulation, with the magnitude of changes increasing with burn severity. In the McKenzie watershed, remote sensing data indicated ET decreases of −31.6 % in 2021, -22.9 % in 2022, and -33.2 % in 2023 in burned areas, relative to the pre-fire period (annual average from October 2011 to September 2020) (Fig. 8a). The SWAT-fire model simulated similar ET reductions, with −28.6 % in 2021, -28.3 % in 2022, and -36.7 % in 2023. In contrast, the SWAT-normal simulations showed minimal changes or remained stable compared to the pre-fire period. Likewise, in the North Santiam watershed, remote sensing data showed ET reductions of −29.8 % in 2021, -26.1 % in 2022, and -56.0 % in 2023 (Fig. 8b). SWAT-fire simulated reductions of −15.7 % in 2021, -11.6 % in 2022, and -23.2 % in 2023, outperforming the SWAT-normal simulation. These findings suggest that the SWAT-fire simulation more accurately represents post-fire ET dynamics and better reflects post-fire hydrologic conditions compared to the SWAT-normal simulation.

Burn severity was negatively associated with simulated ET from the SWAT-fire model in both the McKenzie and North Santiam watersheds (Figs. 9 and 10). In the McKenzie watershed, ET declined more in areas with higher burn severity, with annual reductions ranging from approximately 16 %–39 % across the three post-fire years. The North Santiam watershed showed a similar pattern, with reductions ranging from about 13 % to 32 %. These consistent trends across years and watersheds highlight the strong influence of burn severity on post-fire

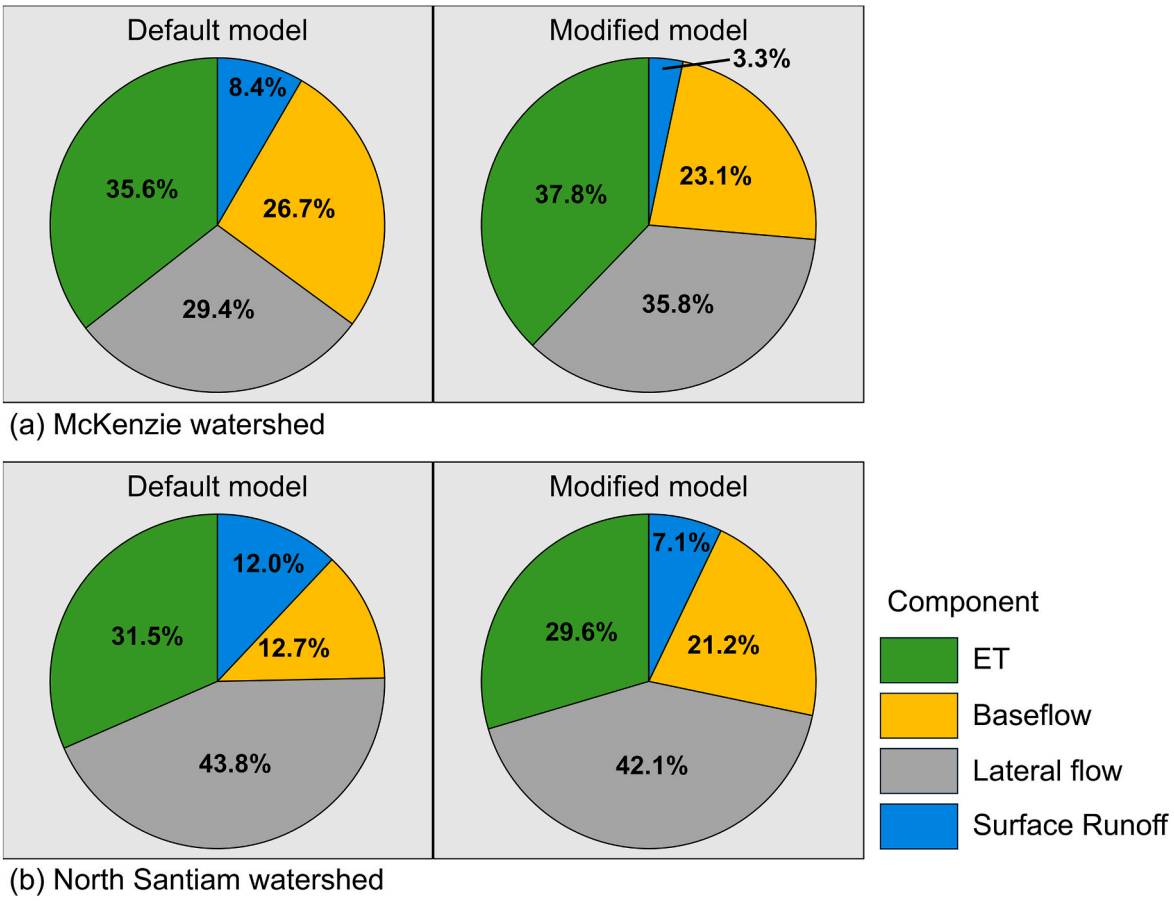

Fig. 4. Average annual water balance under default and improved model parameterization. (a) McKenzie watershed. (b) North Santiam watershed.

ET dynamics.

3.3.2. Water balance partitioning

In the McKenzie River sub-basin, where the burned areas are primarily located in the downstream regions, the water balance in the burned sub-watersheds from the normal simulation is quite different from that of the entire watershed, specifically for the baseflow contribution (Fig. 4a). The SWAT-normal simulation estimated ET accounted for 38.5 %, lateral flow 48.3 %, baseflow 7.5 %, and surface runoff only 5.7 %. The SWAT-fire simulation showed substantial changes: ET sharply decreased to 28.6 %, surface runoff surged to 19.3 %. Lateral flow remained the dominant runoff component (43.6 %), and baseflow showed a slight increase to 8.5 %. These results indicate that wildfire-induced reductions in canopy cover and soil infiltration capacity enhanced surface runoff and reduced ET (Fig. 11a).

In the North Santiam River sub-basin, where burned areas are distributed throughout the entire watershed, the SWAT-normal simulation indicated that ET comprised 38.5 %, lateral flow 45.5 %, baseflow 19.2 %, and surface runoff 7.2 % of the total water balance, which is similar to the water balance composition of the entire watershed (Fig. 4b). However, significant shifts were observed in the SWAT-fire simulation, with ET decreasing to 23.2 %, lateral flow declining 32.1 %, baseflow dropping to 17.3 %, and surface runoff surging to 27.4 %. These results also suggest that wildfires substantially increase surface runoff and decrease ET, altering the primary water balance components (Fig. 11b). The significant increase in surface runoff and a corresponding decrease in ET observed in the SWAT-fire simulations highlight the impacts of fire on water balance partitioning.

4. Discussion

In our study of two burned sub-basins in Oregon, USA, we demonstrated how calibration of the SWAT model for forest and wildfire dynamics improved simulation of seasonal and post-fire hydrological and vegetation fluxes. Our approach resulted in improved simulations of wildfire-induced hydrologic fluxes of seasonal runoff, peak streamflow, water balance, ET, and LAI, which were poorly represented by SWAT simulations that used conventional calibration methods. Moreover, we demonstrate that fire severity-mediated hydrological dynamics can be effectively captured by holistic calibration of SWAT. Our results showed that wildfires redistribute water resources, with reduced vegetation cover contributing to decreased ET and greater runoff. These hydrological alterations could have long-term implications for water availability, flood risk, and ecosystem recovery in post-fire landscapes.

The modified calibration improved hydrological simulations in the forested watersheds, as indicated by enhanced streamflow, ET, and LAI predictions. For instance, the modified model notably corrected seasonal variations ET, closely aligning with remote-sensing observations. In addition, the modified parameterization improved the representation of water balance partitioning by reducing surface runoff and strengthening subsurface contributions, which dominate flow generation in the Cascade catchments. Specifically, in the McKenzie watershed, surface runoff decreased from 8.4 % to 3.3 %, while combined subsurface flow (lateral + baseflow) increased from 56.1 % to 58.9 %. Similarly, in the North Santiam watershed, surface runoff decreased from 12.0 % to 7.1 %, and subsurface flow increased from 56.5 % to 63.3 % (Fig. 4). This improvement in water balance partitioning has significant implications for water resource management, particularly in regions where subsurface contributions influence streamflow. These shifts also underscore the

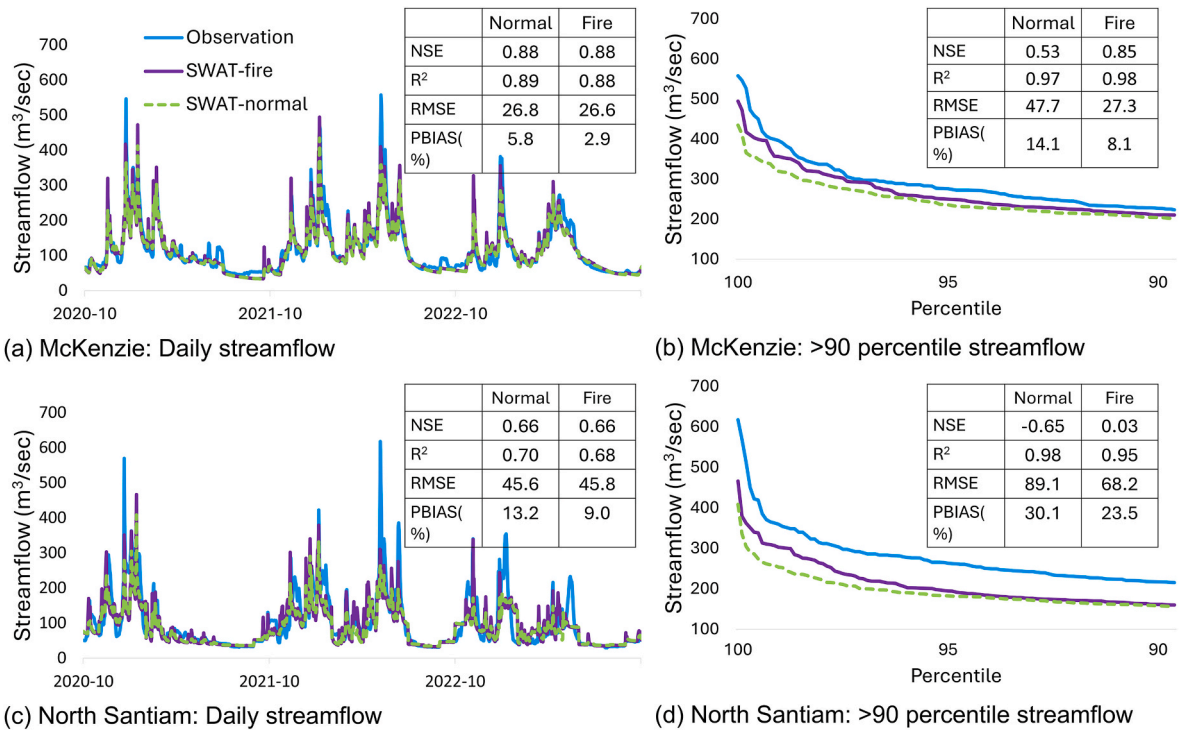

Fig. 5. Comparison of streamflow from USGS observations, SWAT-fire, and SWAT-normal simulations. Blue lines represent USGS observations, purple lines indicate SWAT-fire simulations, and green dashed lines show SWAT-normal simulations. (a) Daily streamflow comparison in the McKenzie watershed at USGS station 14164900. (b) Daily streamflow above the 90th percentile at the same location as (a). (c) Daily streamflow comparison in the North Santiam watershed at USGS station 14183000. (d) Daily streamflow above the 90th percentile at the same location as (c). (For interpretation of the references to colour in this figure legend, the reader is referred to the Web version of this article.)

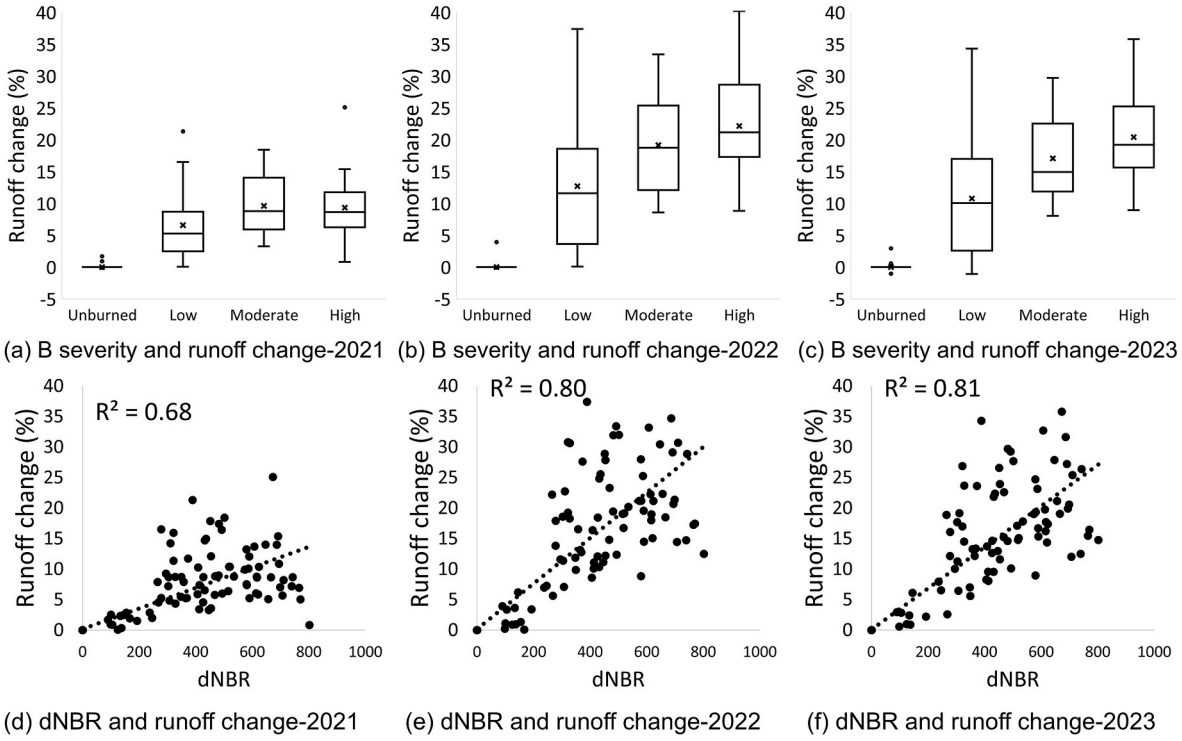

Fig. 6. (a–c) Box and whisker plots showing simulated runoff change (%) of the burned sub-watersheds from SWAT-fire across different burn severities for each post-fire year in the McKenzie watershed (2021–2023). The boxes represent the interquartile range (IQR) with the 25th percentile, median, and 75th percentile values, while the whiskers extend to the minimum and maximum values. The 'x' symbol indicates the mean. (d–f) Scatter plots illustrating the relationship between runoff change and dNBR (Differenced Normalized Burn Ratio) for each post-fire year (2001–2023).

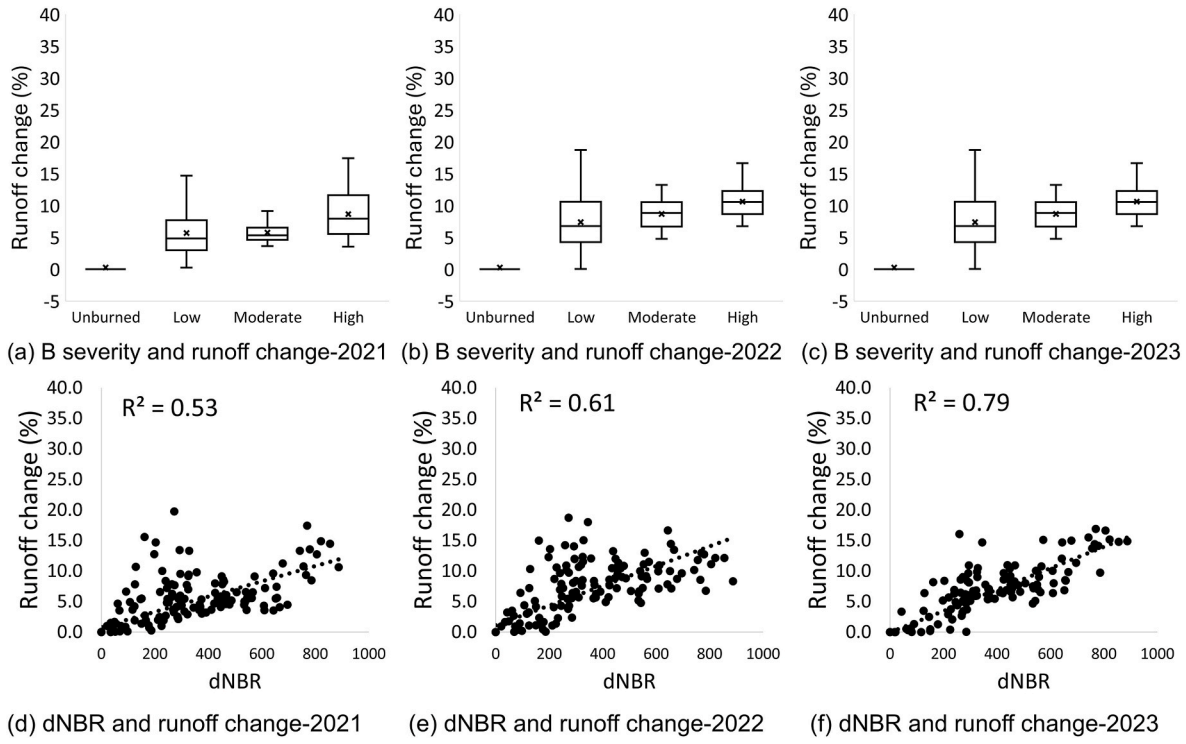

Fig. 7. (a–c) Box and whisker plots showing simulated runoff change (%) of the burned sub-watersheds from SWAT-fire across different burn severities for each post-fire year in the North Santiam watershed. The boxes represent the 25th percentile, median, and 75th percentile values, while the whiskers extend to the minimum and maximum values. The 'x' symbol indicates the mean. (d–f) Scatter plots illustrating the relationship between runoff change and dNBR for each post-fire year.

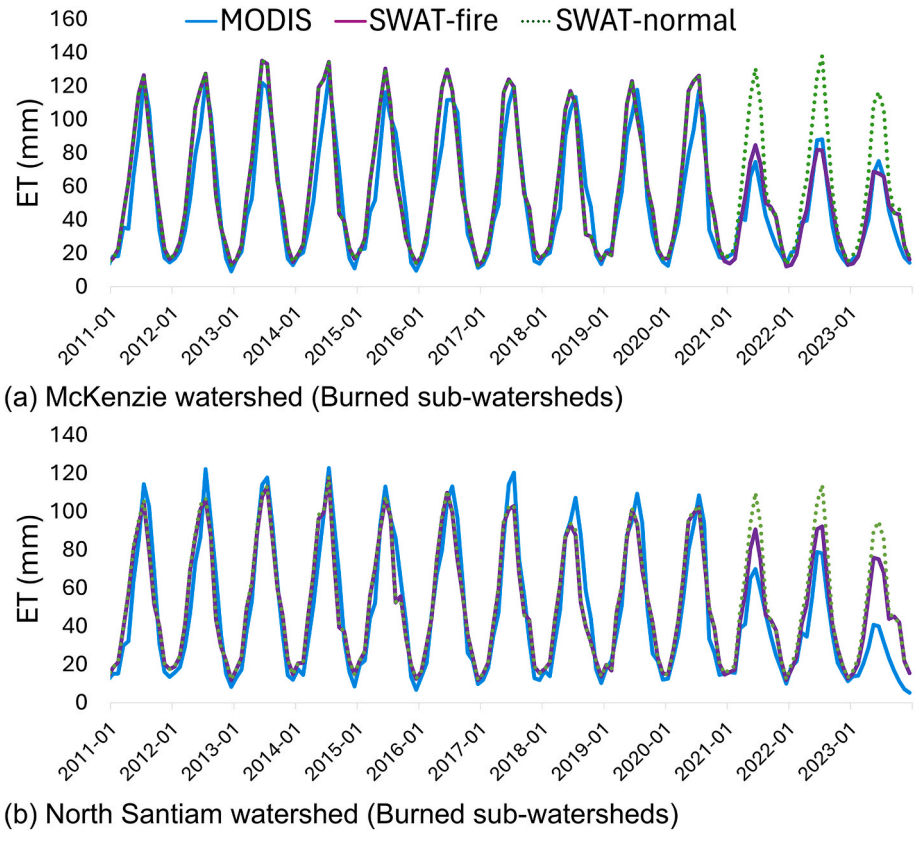

Fig. 8. Comparison of monthly total ET in the burned sub-watersheds based on MODIS observations, SWAT-fire simulations, and SWAT-normal simulations. Blue lines represent MODIS observations, purple lines indicate SWAT-fire simulations, and green dashed lines illustrate SWAT-normal simulations. (a) McKenzie watershed; (b) North Santiam watershed.

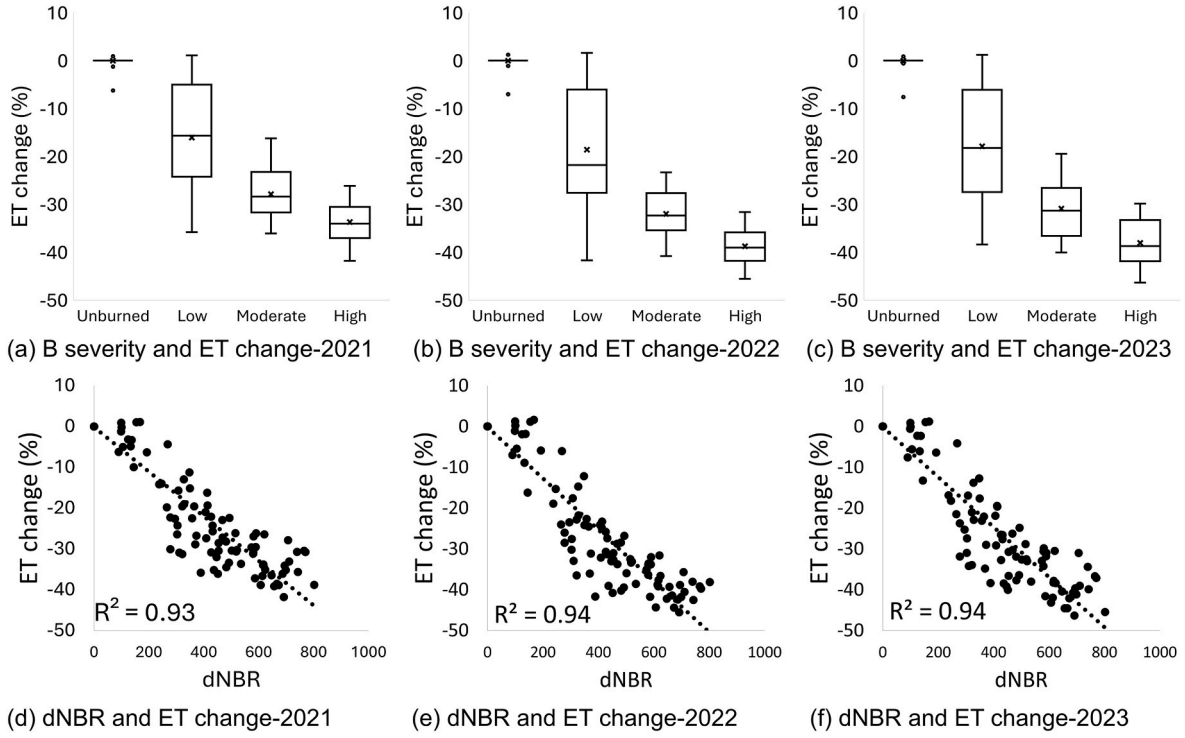

Fig. 9. (a–c) Box and whisker plots showing simulated ET change (%) of the burned sub-watersheds from SWAT-fire across different burn severities for each post-fire year in the McKenzie watershed. The boxes represent the 25th percentile, median, and 75th percentile values, while the whiskers extend to the minimum and maximum values. The 'x' symbol indicates the mean. (d–f) Scatter plots illustrating the relationship between ET change and dNBR for each post-fire year.

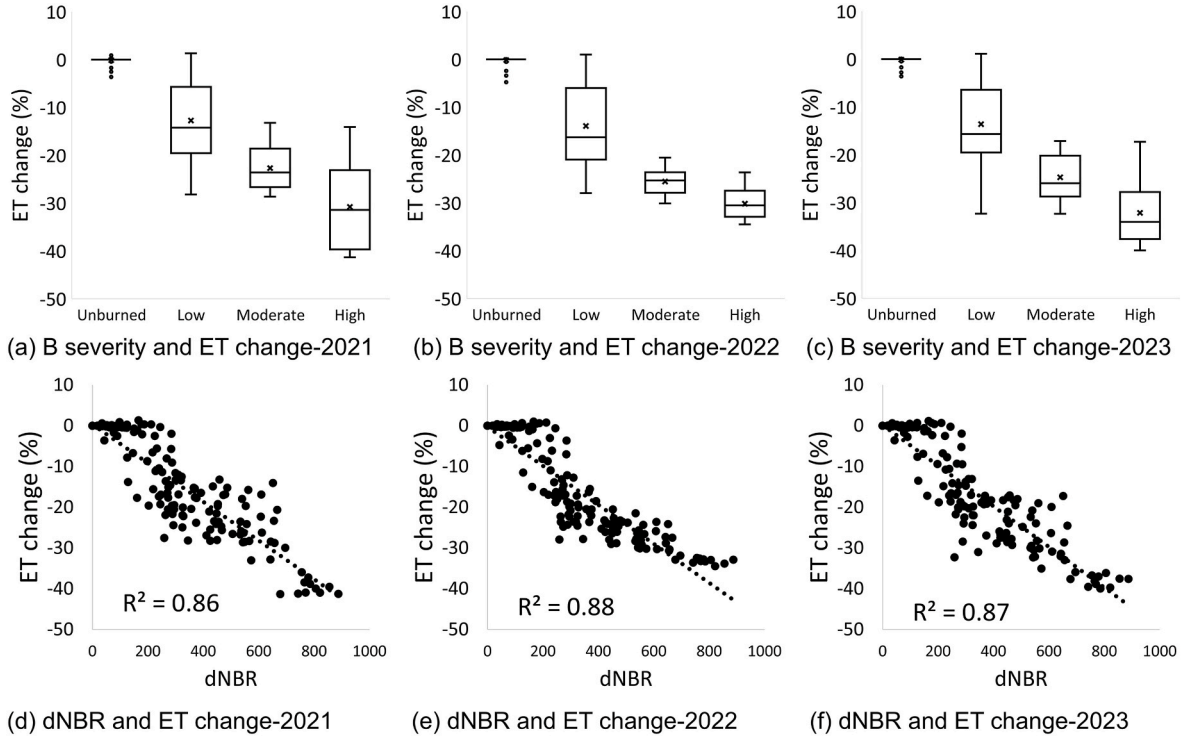

Fig. 10. (a–c) Box and whisker plots showing simulated ET change (%) of the burned sub-watersheds from SWAT-fire across different burn severities for each post-fire year in the North Santiam watershed. The boxes represent the 25th percentile, median, and 75th percentile values, while the whiskers extend to the minimum and maximum values. The 'x' symbol indicates the mean. (d–f) Scatter plots illustrating the relationship between ET change and dNBR for each post-fire year.

importance of interpreting subsurface contributions within an appropriate hydrologic framework.

In SWAT, lateral flow and baseflow are represented as distinct components, whereas many hydrologic studies define baseflow more broadly as the portion of streamflow sustained by groundwater and other delayed subsurface pathways, including contributions from

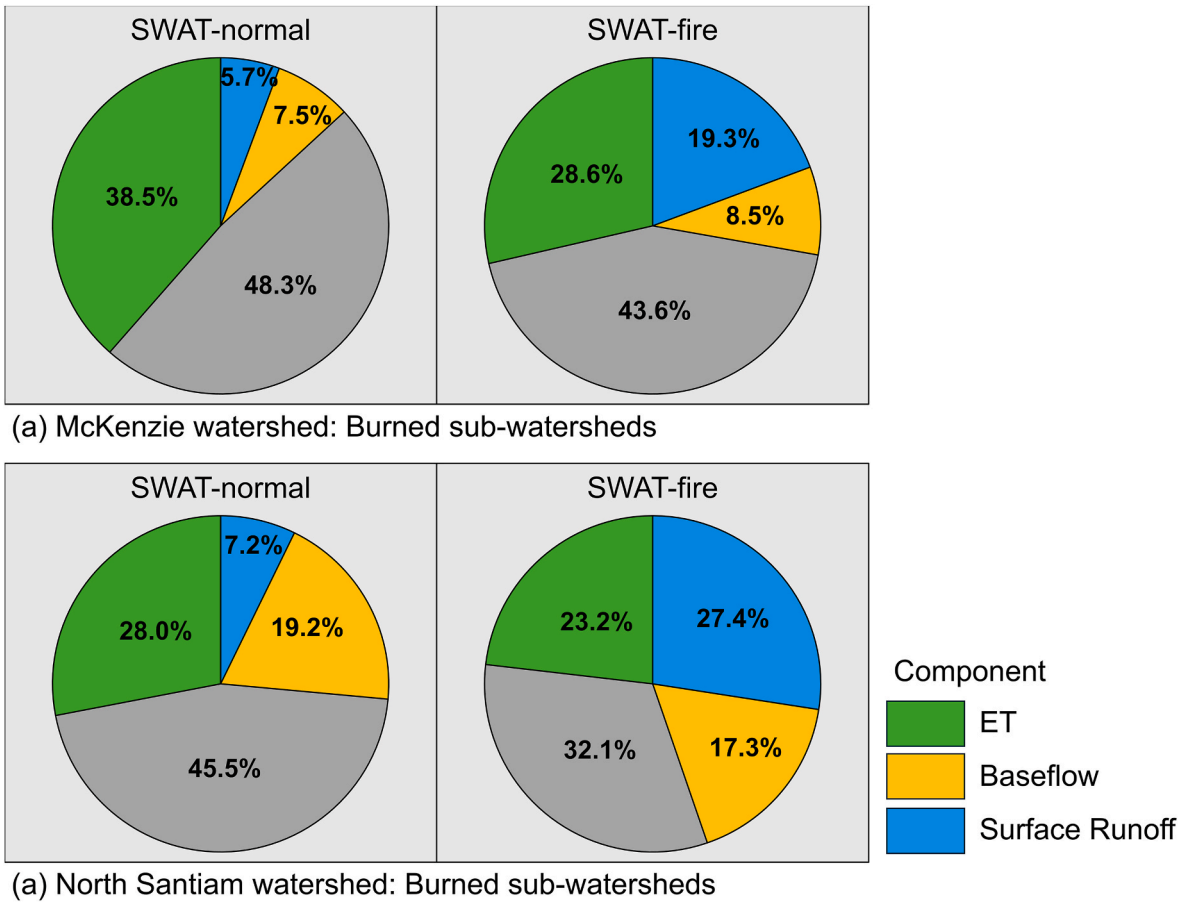

Fig. 11. Average annual water balance under the SWAT-normal and SWAT-fire simulations during the post-fire years (October 2020 to September 2023) in the burned sub-watersheds. (a) McKenzie watershed. (b) North Santiam watershed.

interflow (Price, 2011; Singh et al., 2019; Stoelzle et al., 2020). This difference in terminology highlights that subsurface pathways are not always conceptualized consistently across modeling and observational studies. Consequently, this broader usage can cause confusion in distinguishing lateral and groundwater contributions. Recent modeling studies further showed that shallow subsurface pathways, including lateral flow, can play a dominant role in streamflow generation in geologically complex or steep terrains (Sánchez-Gómez et al., 2024), illustrating that lateral contributions can be substantial under certain landscape conditions. These insights are important for interpreting our water-balance results because the study watersheds are located in the western Cascades, where steep topography and shallow flow paths strongly influence runoff generation. In our study basins, subsurface processes exert a major influence on total streamflow, with lateral flow contributing substantially to the overall subsurface component. This interpretation aligns with conceptual hydrologic understanding of the western Cascades, where subsurface pathways frequently play an important role in flow generation (McGuire and McDonnell, 2010). Based on the modified calibration and the SWAT-fire simulation, we demonstrated post-fire hydrologic dynamics, including increased runoff, elevated streamflow, and reduced ET. Specifically, the SWAT-fire simulation accurately captured notable reductions in ET and improved simulations of high streamflow events, highlighting the sensitivity of hydrologic responses to fire-induced parameter adjustments. We also found that those hydrological changes were strongly related to fire severity, reinforcing conclusions from previous studies.

Our findings are consistent with several previous studies, including Kang et al. (2024), who reported substantial ET reductions and increased runoff post-wildfire using remote sensing and field-based observations. Similarly, Wampler et al. (2023) observed increases in post-fire streamflow, which was correlated with burn severity, underscoring the critical role of vegetation loss in altering hydrological regimes. Other studies have also observed greater reductions in ET and increases in runoff in watersheds burned at high severity compared to lower severity burns (Hallema et al., 2018; Wine et al., 2018). These results emphasized the critical role of fire severity in mediating post-fire hydrological responses. Moreover, our results emphasized the importance of careful representation of burn severity to accurately predict the magnitude of hydrological responses in post-fire hydrological modeling. Integrating these insights into hydrological models, such as SWAT-fire, can enhance predictive capabilities for forested watersheds impacted by wildfire events.

Despite these methodological advancements, several uncertainties remain in the wildfire simulation. The wildfire module simplified complex post-fire processes, including changes in soil hydraulic properties and evolving surface characteristics. Recent studies have highlighted the complexity of wildfire-induced alterations in soil properties based on field observations, revealing inconsistencies with our study. For instance, Pimont (2024) reported no notable differences in soil hydraulic properties across burn severities in the Pacific Northwest, but unexpected increases in hydraulic conductivity were found in the burned areas. These findings contrasted with our model assumptions, which anticipated increased runoff due to reduced infiltration capacity after wildfires, highlighting limitations in current modeling frameworks and the need for improved post-fire soil hydraulic information.

Moreover, ET calibration was conducted with remote sensing observations that have limitations in capturing site-specific variability. For example, MODIS ET products may underestimate actual ET in densely

forested regions (Mu et al., 2011). The accuracy of remote sensing-based ET estimates potentially affect model calibration outcomes. While the modified model generated better ET simulations compared to the default model, uncertainties in ET observations and post-fire vegetation responses remain important factors influencing the accuracy of hydrologic predictions. Addressing these limitations through long-term monitoring and improved parameterization considering vegetation recovery would enhance future wildfire-hydrology modeling efforts.

The temporal scale of our study, spanning three years post-fire, provided valuable insights into immediate hydrologic responses but represented only the initial stages of hydrologic recovery. Post-fire recovery trajectories typically extended over multiple years or even decades (Ebel et al., 2022; Holden et al., 2012; Niemeyer et al., 2020). Thus, our simulations likely captured only the initial hydrological responses and may not fully reflect longer-term recovery processes involving vegetation regrowth, soil structure stabilization, and ecosystem recovery dynamics. Ebel et al. (2022) provided a comprehensive framework for assessing hydrologic recovery, emphasizing evaluating multiple metrics, such as soil infiltration, vegetation cover, runoff generation, and channel responses over varying temporal scales. Their study highlighted the complexity and variability inherent in hydrologic recovery, suggesting that vegetation regrowth rates, management practices, and regional climatic conditions influence recovery trajectories. Furthermore, climatic variability, management practices, and other landscape disturbances occurring concurrently or after wildfires can significantly influence hydrologic responses to wildfires.

In addition, our study primarily examined immediate post-fire hydrologic impacts and did not explicitly incorporate the potential interactive effects of climate variability, such as droughts or unusually wet conditions, nor management interventions like salvage logging and reforestation efforts. Previous studies have highlighted that these factors significantly influence hydrologic responses following wildfires (Ebel et al., 2022; Wagenbrenner et al., 2021). A key advancement from our work is developing a robust model calibration approach, which can be leveraged to investigate these longer-term effects and their interactions with climatic variables and management strategies. Incorporating these considerations in future modeling will enhance our understanding of watershed dynamics post-fire and improve predictive accuracy. Although this study utilized SWAT 2012, the calibration framework and wildfire-specific parameter adjustment presented here are compatible with the structure of SWAT+, which includes enhanced spatial representation and the capacity to simulate fire operations through its land management module (Bieger et al., 2017). Future work integrating these approaches into SWAT + would allow for a more flexible and process-oriented simulation of post-fire hydrologic dynamics across interconnected landscape units.

Finally, our current wildfire simulation utilized fixed adjusting parameters for the entire post-fire period, which may not always be realistic. Some studies have shown that post-fire processes, such as debris flows, primarily occur within the first year following wildfire. For instance, DeGRAFF et al. (2015) reported that the majority (85 %) of debris flows occurred within 12 months post-fire, with 71 % within the first six months. Similarly, Santi and Morandi (2013) noted that debris flows from burned areas predominantly occurred within the first year. Their findings suggested that the adjusted parameters should ideally be dynamic rather than static over time to represent post-fire watershed dynamics accurately.

5. Conclusion

In our study, we used a modified calibration technique that incorporated a more explicit forest and wildfire module into SWAT to improve simulation of post-fire hydrologic responses in our study watersheds in Oregon, USA. By calibrating the model for ET fluxes and recovery of LAI in forest ecosystems, in conjunction with streamflow, SWAT was able to provide a more accurate depiction of wildfire severity effects on water balance and hydrological dynamics. Our model simulations performed well at representing the variability in decreased ET and corresponding increases in streamflow that were generally driven by differences in burn severity. As such, our model outputs were generally consistent with observations from the study watersheds.

These findings are particularly relevant in regions like the Pacific Northwest, where large, high severity wildfires are occurring more frequently. The improved accuracy of these simulations can inform water and forest managers in wildfire-prone regions, providing them with valuable tools for better planning and mitigation strategies, such as evaluating future wildfire scenarios and refining region-specific management strategies based on projected climate and fire severity changes. Anticipating changes in ET and streamflow after wildfire would help to develop more proactive responses to protect water resources, enhance ecosystem recovery, and reduce the risks associated with wildfire impacts on water supply and quality.

CRediT authorship contribution statement

Hyunwoo Kang: Writing – review & editing, Writing – original draft, Visualization, Validation, Methodology, Investigation, Formal analysis, Data curation, Conceptualization. **Cameron E. Naficy:** Writing – review & editing, Validation, Project administration, Methodology, Funding acquisition, Conceptualization. **Kevin D. Bladon:** Writing – review & editing, Validation, Resources, Project administration, Methodology, Funding acquisition, Conceptualization.

Software and data availability

- Name of software: Soil and Water Assessment Tool (SWAT)
- Developers: United States Department of Agriculture (USDA), Agricultural Research Service (Dr. Jeff Arnold)
- Year first available: 1998
- Contact: https://swat.tamu.edu/support/
- Cost: Free
- Program language: Fortran
- Software availability and source code: https://swat.tamu.edu/software/swat/
- Documentation: Detailed documentation for application installation, testing, and deployment can be found at https://swat.tamu.edu/
- Data availability:
  - The observed streamflow data can be downloaded free of charge from the United States Geological Survey (USGS) National Water Information System (NWIS) at: https://waterdata.usgs.gov/nwis.
    The specific stream gage sites used in this study are publicly accessible and were selected based on data availability and proximity to the study watersheds.
  - The MODIS evapotranspiration (ET) data used for model calibration are freely available from the NASA Earthdata portal: https://lpdaac.usgs.gov/products/mod16a2v061/
    The MOD16A2 Version 6 dataset provides 8-day composite ET estimates at 500 m resolution globally.
  - The MODIS Leaf Area Index (LAI) data used in the analysis can be downloaded from NASA's LP DAAC: https://lpdaac.usgs.gov/products/mcd15a2hv061/.
  - The burn severity data based on differenced Normalized Burn Ratio (dNBR) were obtained from the Monitoring Trends in Burn Severity (MTBS) project at: https://www.mtbs.gov.
    MTBS provides standardized burn severity maps for large wildfires across the United States.

Declaration of competing interest

The authors declare that they have no known competing financial interests or personal relationships that could have appeared to influence the work reported in this paper.

Acknowledgements

This project was supported by a Cooperative Agreement (UWSC13136) from the U.S. Geological Survey Northwest Climate Adaptation Science Center to CEN. Its contents are solely the responsibility of the authors and do not necessarily represent the views of the Northwest Climate Adaptation Science Center or the USGS. Additional funding was provided by the U.S. Forest Service, United States (agreement number 22-JV-11261952-071). This manuscript is submitted for publication with the understanding that the United States Government is authorized to reproduce and distribute reprints for Governmental purposes.

Declaration of AI writing assistant: During the preparation of this work, the first author (Hyunwoo Kang) used ChatGPT in some part of manuscript to improve readability and grammar refinement. After using this tool, all authors thoroughly reviewed and edited the content as needed and took full responsibility for the published article.

Appendix A. Supplementary data

Supplementary data to this article can be found online at https://doi.org/10.1016/j.envsoft.2026.106896.

References

Abatzoglou, J.T., Rupp, D.E., O'Neill, L.W., Sadegh, M., 2021. Compound extremes drive the Western Oregon wildfires of September 2020. Geophys. Res. Lett. 48. https://doi.org/10.1029/2021GL092520 e2021GL092520.

Abbaspour, K.C., 2014. SWAT-CUP 2012: SWAT Calibration and Uncertainty programs—A User Manual: Swiss Federal Institute of Aquatic Science and Technology.

Abbaspour, K.C., Rouholahnejad, E., Vaghefi, S., Srinivasan, R., Yang, H., Kløve, B., 2015. A continental-scale hydrology and water quality model for Europe: calibration and uncertainty of a high-resolution large-scale SWAT model. J. Hydrol. 524, 733–752. https://doi.org/10.1016/j.jhydrol.2015.03.027.

Arnold, J.G., Srinivasan, R., Muttiah, R.S., Williams, J.R., 1998. Large area hydrologic modeling and assessment part I: model Development1. JAWRA J. Am. Water Resour. Assoc. 34, 73–89. https://doi.org/10.1111/j.1752-1688.1998.tb05961.x.

Bart, R.R., Kennedy, M.C., Tague, C.L., McKenzie, D., 2020. Integrating fire effects on vegetation carbon cycling within an ecohydrologic model. Ecol. Model. 416, 108880. https://doi.org/10.1016/j.ecolmodel.2019.10888.

Basso, M., Vieira, D.C.S., Ramos, T.B., Mateus, M., 2020. Assessing the adequacy of SWAT model to simulate postfire effects on the watershed hydrological regime and water quality. Land Degrad. Dev. 31, 619–631. https://doi.org/10.1002/ldr.3476.

Bieger, K., Arnold, J.G., Rathjens, H., White, M.J., Bosch, D.D., Allen, P.M., Volk, M., Srinivasan, R., 2017. Introduction to SWAT+, a completely restructured version of the soil and water assessment tool. JAWRA J. Am. Water Resour. Assoc. 53, 115–130. https://doi.org/10.1111/1752-1688.12482.

Bladon, K.D., Emelko, M.B., Silins, U., Stone, M., 2014. Wildfire and the future of water supply. Environ. Sci. Technol. 48, 8936–8943. https://doi.org/10.1021/es500130g.

Collar, N.M., Saxe, S., Rust, A.J., Hogue, T.S., 2021. A CONUS-scale study of wildfire and evapotranspiration: spatial and temporal response and controlling factors. J. Hydrol. 603, 127162. https://doi.org/10.1016/j.jhydrol.2021.127162.

Dangol, S., Zhang, X., Liang, X.-Z., Anderson, M., Crow, W., Lee, S., Moglen, G.E., McCarty, G.W., 2023. Multivariate calibration of the SWAT model using remotely sensed datasets. Remote Sens. 15, 2417. https://doi.org/10.3390/rs15092417.

DeGRAFF, J.V., Cannon, S.H., Gartner, J.E., 2015. The timing of susceptibility to post-fire debris flows in the Western United States. Environ. Eng. Geosci. 21, 277–292. https://doi.org/10.2113/gseegeosci.21.4.277.

Devkota, N., Lamichhane, S., Bhattarai, P.K., 2024. Multi-site calibration of the SWAT hydrological model and study of spatio-temporal variation of water balance components in the Narayani River basin, central part of Nepal. H2Open J. 7, 114–129. https://doi.org/10.2166/h2oj.2024.084.

Dewitz, J., USGS, 2021. National Land Cover Database (NLCD) 2019 products (ver. 3.0, February 2024). U.S. Geol. Survey data release.

Dobre, M., Srivastava, A., Lew, R., Deval, C., Brooks, E.S., Elliot, W.J., Robichaud, P.R., 2022. WEPPcloud: an online watershed-scale hydrologic modeling tool. Part II. Model performance assessment and applications to forest management and wildfires. J. Hydrol. 610, 127776. https://doi.org/10.1016/j.jhydrol.2022.127776.

Ebel, B.A., Moody, J.A., 2020. Parameter estimation for multiple post-wildfire hydrologic models. Hydrol. Process. 34, 4049–4066. https://doi.org/10.1002/hyp.13865.

Ebel, B.A., Moody, J.A., Martin, D.A., 2012. Hydrologic conditions controlling runoff generation immediately after wildfire. Water Resour. Res. 48. https://doi.org/10.1029/2011WR011470.

Ebel, B.A., Wagenbrenner, J.W., Kinoshita, A.M., Bladon, K.D., 2022. Hydrologic recovery after wildfire: a framework of approaches, metrics, criteria, trajectories, and timescales. J. Hydrol. Hydromechanics 70, 388–400. https://doi.org/10.2478/johh-2022-0033.

Ebel, B.A., Shephard, Z.M., Walvoord, M.A., Murphy, S.F., Partridge, T.F., Perkins, K.S., 2023. Modeling post-wildfire hydrologic response: review and future directions for applications of physically based distributed simulation. Earths Future 11. https://doi.org/10.1029/2022EF003038 e2022EF003038.

Elliot, W.J., 2004. Wepp internet interfaces for forest erosion Prediction 1. JAWRA J. Am. Water Resour. Assoc. 40, 299–309. https://doi.org/10.1111/j.1752-1688.2004.tb01030.x.

Emmerton, C.A., Cooke, C.A., Hustins, S., Silins, U., Emelko, M.B., Lewis, T., Kruk, M.K., Taube, N., Zhu, D., Jackson, B., Stone, M., Kerr, J.G., Orwin, J.F., 2020. Severe Western Canadian wildfire affects water quality even at large basin scales. Water Res. 183, 116071. https://doi.org/10.1016/j.watres.2020.116071.

Geological Survey, U.S., 2022. 1 Arc-second digital elevation models (DEMs). at URL. https://data.usgs.gov/datacatalog/data/USGS:35f9c4d4-b113-4c8d-8691-47c428c29a5b. (Accessed 19 October 2022).

González-Pelayo, O., Prats, S.A., van den Elsen, E., Malvar, M.C., Ritsema, C., Bautista, S., Keizer, J.J., 2024. The effects of wildfire frequency on post-fire soil surface water dynamics. Eur. J. For. Res. 143, 493–508. https://doi.org/10.1007/s10342-023-01635-z.

Haas, H., Kalin, L., Srivastava, P., 2022a. Improved forest dynamics leads to better hydrological predictions in watershed modeling. Sci. Total Environ. 821, 153180. https://doi.org/10.1016/j.scitotenv.2022.153180.

Haas, H., Reaver, N.G.F., Karki, R., Kalin, L., Srivastava, P., Kaplan, D.A., Gonzalez-Benecke, C., 2022b. Improving the representation of forests in hydrological models. Sci. Total Environ. 812, 151425. https://doi.org/10.1016/j.scitotenv.2021.151425.

Hallema, D.W., Sun, G., Caldwell, P.V., Norman, S.P., Cohen, E.C., Liu, Y., Ward, E.J., McNulty, S.G., 2017. Assessment of wildland fire impacts on watershed annual water yield: analytical framework and case studies in the United States. Ecohydrology 10, e1794. https://doi.org/10.1002/eco.1794.

Hallema, D.W., Sun, G., Caldwell, P.V., Norman, S.P., Cohen, E.C., Liu, Y., Bladon, K.D., McNulty, S.G., 2018. Burned forests impact water supplies. Nat. Commun. 9, 1307. https://doi.org/10.1038/s41467-018-03735-6.

Hanan, E.J., Ren, J., Tague, C.L., Kolden, C.A., Abatzoglou, J.T., Bart, R.R., Kennedy, M. C., Liu, M., Adam, J.C., 2021. How climate change and fire exclusion drive wildfire regimes at actionable scales. Environ. Res. Lett. 16, 024051. https://doi.org/10.1088/1748-9326/abd78e.

Her, Y., Frankenberger, J., Chaubey, I., Srinivasan, R., 2015. Threshold effects in HRU definition of the soil and water assessment tool. Trans. ASABE 58, 367–378.

Holden, Z.A., Luce, C.H., Crimmins, M.A., Morgan, P., 2012. Wildfire extent and severity correlated with annual streamflow distribution and timing in the Pacific Northwest, USA (1984–2005). Ecohydrology 5, 677–684. https://doi.org/10.1002/eco.257.

Jefferson, A., Grant, G., Rose, T., 2006. Influence of volcanic history on groundwater patterns on the west slope of the Oregon high cascades. Water Resour. Res. 42. https://doi.org/10.1029/2005WR004812.

Kang, H., Cole, R.P., Miralha, L., Compton, J.E., Bladon, K.D., 2024. Hydrologic responses to wildfires in Western Oregon, USA. J. Hydrol. 639, 131612. https://doi.org/10.1016/j.jhydrol.2024.131612.

Keeley, J.E., 2009. Fire intensity, fire severity and burn severity: a brief review and suggested usage. Int. J. Wildland Fire 18, 116–126. https://doi.org/10.1071/WF07049.

Key, C.H., Benson, N.C., 2006. Landscape Assessment: Ground Measure of Severity, the Composite Burn Index; and Remote Sensing of Severity, the Normalized Burn Ratio. (FIREMON: Fire Effects Monitoring and Inventory System.). USDA Forest Service, Rocky Mountain Research Station, Ogden, UT.

Kiesel, J., Schmalz, B., Brown, G.L., Fohrer, N., 2013. Application of a hydrological-hydraulic modelling cascade in lowlands for investigating water and sediment fluxes in catchment, channel and reach. J. Hydrol. Hydromechanics 61, 334–346.

Koltsida, E., Kallioras, A., 2022. Multi-variable SWAT model calibration using satellite-based evapotranspiration data and streamflow. Hydrology 9, 112. https://doi.org/10.3390/hydrology9070112.

Kraus, T.E.C., Anderson, C.A., Morgenstern, K., Downing, B.D., Pellerin, B.A., Bergamaschi, B.A., 2010. Determining sources of dissolved organic carbon and disinfection byproduct precursors to the McKenzie river, Oregon. J. Environ. Qual. 39, 2100–2112. https://doi.org/10.2134/jeq2010.0030.

Lai, G., Luo, J., Li, Q., Qiu, L., Pan, R., Zeng, X., Zhang, L., Yi, F., 2020. Modification and validation of the SWAT model based on multi-plant growth mode, a case study of the Meijiang River basin, China. J. Hydrol. 585, 124778. https://doi.org/10.1016/j.jhydrol.2020.124778.

Lee, S., Kim, D., McCarty, G.W., Anderson, M., Gao, F., Lei, F., Moglen, G.E., Zhang, X., Yen, H., Qi, J., Crow, W., 2024. Spatial calibration and uncertainty reduction of the SWAT model using multiple remotely sensed data. Heliyon 10, e30923. https://doi.org/10.1016/j.heliyon.2024.e30923.

Li, Z., Li, B., Jiang, P., Hammond, G.E., Shuai, P., Coon, E., Chen, X., 2023. Evaluating the Effects of Burn Severity and Precipitation on Post-fire Watershed Responses Using Distributed Hydrologic Models.

Loiselle, D., Du, X., Alessi, D.S., Bladon, K.D., Faramarzi, M., 2020. Projecting impacts of wildfire and climate change on streamflow, sediment, and organic carbon yields in a forested watershed. J. Hydrol. 590, 125403. https://doi.org/10.1016/j.jhydrol.2020.125403.

Long, W.B., Chang, H., 2022. Event scale analysis of streamflow response to wildfire in Oregon, 2020. Hydrology 9, 157. https://doi.org/10.3390/hydrology9090157.

Ma, Q., Bales, R.C., Rungee, J., Conklin, M.H., Collins, B.M., Goulden, M.L., 2020. Wildfire controls on evapotranspiration in California's Sierra Nevada. J. Hydrol. 590, 125364. https://doi.org/10.1016/j.jhydrol.2020.125364.

McGuire, K.J., McDonnell, J.J., 2010. Hydrological connectivity of hillslopes and streams: characteristic time scales and nonlinearities. Water Resour. Res. 46. https://doi.org/10.1029/2010WR009341.

Moody, J.A., Ebel, B.A., Nyman, P., Martin, D.A., Stoof, C., McKinley, R., 2015. Relations between soil hydraulic properties and burn severity. Int. J. Wildland Fire 25, 279–293. https://doi.org/10.1071/WF14062.
MTBS, 2024. Monitoring trends in burn severity (MTBS). URL. https://www.mtbs.gov/. (Accessed 19 August 2024).
Mu, Q., Zhao, M., Running, S.W., 2011. Improvements to a MODIS global terrestrial evapotranspiration algorithm. Remote Sens. Environ. 115, 1781–1800. https://doi.org/10.1016/j.rse.2011.02.019.
Myneni, R., Knyazikhin, Y., Park, T., 2015. MOD15A2H MODIS/Terra leaf area Index/FPAR 8-Day L4 global 500m SIN grid V006. NASA EOSDIS Land Processes DAAC.
Narsimlu, B., Gosain, A.K., Chahar, B.R., Singh, S.K., Srivastava, P.K., 2015. SWAT model calibration and uncertainty analysis for streamflow prediction in the Kunwari River basin, India, using sequential uncertainty fitting. Environ. Processes 2, 79–95. https://doi.org/10.1007/s40710-015-0064-8.
Nash, J.E., Sutcliffe, J.V., 1970. River flow forecasting through conceptual models part I — a discussion of principles. J. Hydrol. 10, 282–290. https://doi.org/10.1016/0022-1694(70)90255-6.
Natural Resources Conservation Service (NRCS), 2025. United States department of agriculture. Web Soil Survey. http://websoilsurvey.nrcs.usda.gov/. (Accessed 4 October 2025).
Neitsch, S.L., Arnold, J.G., Kiniry, J.R., Williams, J.R., 2011. Soil and Water Assessment Tool Theoretical Documentation Version 2009 (No. No. 406). Texas Water Resources Institute Technical Report. Texas A & M University System, College Station, TX.
Niemeyer, R.J., Bladon, K.D., Woodsmith, R.D., 2020. Long-term hydrologic recovery after wildfire and post-fire forest management in the interior Pacific northwest. Hydrol. Process. 34, 1182–1197. https://doi.org/10.1002/hyp.13665.
Oregon Department of Forestry, 2022. Forest Facts, 2020 Labor Day Fires: Post-Fire Challenges with Invasive Plants.
Parajuli, P.B., Jayakody, P., Ouyang, Y., 2018. Evaluation of using remote sensing evapotranspiration data in SWAT. Water Resour. Manag. 32, 985–996. https://doi.org/10.1007/s11269-017-1850-z.
Pimont, C., 2024. Effects of Wildfire on Soil Hydraulic Properties in the Western Oregon Cascades. Oregon State University.
Poon, P.K., Kinoshita, A.M., 2018. Spatial and temporal evapotranspiration trends after wildfire in semi-arid landscapes. J. Hydrol. 559, 71–83. https://doi.org/10.1016/j.jhydrol.2018.02.023.
Price, K., 2011. Effects of watershed topography, soils, land use, and climate on baseflow hydrology in humid regions: a review. Prog. Phys. Geogr. 35, 465–492. https://doi.org/10.1177/0309133311402711.
PRISM Climate Group, 2022. PRISM 30 Years Precipitation Data (4Km).
Robinne, F.-N., Hallema, D.W., Bladon, K.D., Buttle, J.M., 2020. Wildfire impacts on hydrologic ecosystem services in North American high-latitude forests: a scoping review. J. Hydrol. 581, 124360. https://doi.org/10.1016/j.jhydrol.2019.124360.
Running, S., Mu, Q., Zhao, M., 2017. Mod16a2 modis/terra net evapotranspiration 8-day l4 global 500m sin grid v006. NASA EOSDIS Land Processes DAAC 6.
Sánchez-Gómez, A., Schürz, C., Molina-Navarro, E., Bieger, K., 2024. Groundwater modelling in SWAT+: considerations for a realistic baseflow simulation. Groundw. Sustain. Dev. 26, 101275. https://doi.org/10.1016/j.gsd.2024.101275.
Santi, P.M., Morandi, L., 2013. Comparison of debris-flow volumes from burned and unburned areas. Landslides 10, 757–769. https://doi.org/10.1007/s10346-012-0354-4.
Saxe, S., Hogue, T.S., Hay, L., 2018. Characterization and evaluation of controls on post-fire streamflow response across Western US watersheds. Hydrol. Earth Syst. Sci. 22, 1221–1237. https://doi.org/10.5194/hess-22-1221-2018.
Singh, S.K., Pahlow, M., Booker, D.J., Shankar, U., Chamorro, A., 2019. Towards baseflow index characterisation at national scale in New Zealand. J. Hydrol. 568, 646–657. https://doi.org/10.1016/j.jhydrol.2018.11.025.
Snyder, K.U., Sullivan, T.J., Raymond, R.B., Moore, D., 2002. North Santiam River Watershed Assessment. E&S Environmental Chemistry. Inc., Corvallis, OR.
Spencer, S.A., Winkler, R.D., 2024. Changes in snow-dominated streamflow quantity and timing following an extensive wildfire in British Columbia. Hydrol. Process. 38, e15278. https://doi.org/10.1002/hyp.15278.
Stevens, J.T., Boisramé, G.F.S., Rakhmatulina, E., Thompson, S.E., Collins, B.M., Stephens, S.L., 2020. Forest vegetation change and its impacts on soil water following 47 years of managed wildfire. Ecosystems 23, 1547–1565. https://doi.org/10.1007/s10021-020-00489-5.
Stoelzle, M., Schuetz, T., Weiler, M., Stahl, K., Tallaksen, L.M., 2020. Beyond binary baseflow separation: a delayed-flow index for multiple streamflow contributions. Hydrol. Earth Syst. Sci. 24, 849–867. https://doi.org/10.5194/hess-24-849-2020.
Stoof, C.R., Vervoort, R.W., Iwema, J., van den Elsen, E., Ferreira, A.J.D., Ritsema, C.J., 2012. Hydrological response of a small catchment burned by experimental fire. Hydrol. Earth Syst. Sci. 16, 267–285. https://doi.org/10.5194/hess-16-267-2012.
Tague, C.L., Band, L.E., 2004. RHESSys: regional hydro-ecologic simulation system—an object-oriented approach to spatially distributed modeling of carbon, water, and nutrient cycling. Earth Interact. 8, 1–42. https://doi.org/10.1175/1087-3562(2004)8<1:RRHSSO>2.0.CO;2.
Tague, C., Grant, G.E., 2004. A geological framework for interpreting the low-flow regimes of Cascade streams, Willamette River basin, Oregon. Water Resour. Res. 40. https://doi.org/10.1029/2003WR002629.
Thornton, M.M., Shrestha, R., Wei, Y., Thornton, P.E., Kao, S.-C., Wilson, B.E., 2022. Daymet: Daily Surface Weather Data on a 1-km Grid for North America. Version 4 R1.
Tobin, K.J., Bennett, M.E., 2017. Constraining SWAT calibration with remotely sensed evapotranspiration data. JAWRA J. Am. Water Resour. Assoc. 53, 593–604. https://doi.org/10.1111/1752-1688.12516.
U.S. Army Corps of Engineers, 2025. Dataquery 2.0: query timeseries from USACE Northwestern division. https://www.nwd.usace.army.mil/CRWM/. (Accessed 4 August 2025).
Wagenbrenner, J.W., Ebel, B.A., Bladon, K.D., Kinoshita, A.M., 2021. Post-wildfire hydrologic recovery in mediterranean climates: a systematic review and case study to identify current knowledge and opportunities. J. Hydrol. 602, 126772. https://doi.org/10.1016/j.jhydrol.2021.126772.
Wampler, K.A., Bladon, K.D., Faramarzi, M., 2023. Modeling wildfire effects on streamflow in the Cascade Mountains, Oregon, USA. J. Hydrol. 621, 129585. https://doi.org/10.1016/j.jhydrol.2023.129585.
White, J.T., Fienen, M.N., Barlow, P.M., Welter, D.E., 2018. A tool for efficient, model-independent management optimization under uncertainty. Environ. Model. Software 100, 213–221. https://doi.org/10.1016/j.envsoft.2017.11.019.
Williams, C.H.S., Silins, U., Spencer, S.A., Wagner, M.J., Stone, M., Emelko, M.B., 2019. Net precipitation in burned and unburned subalpine forest stands after wildfire in the Northern Rocky Mountains. Int. J. Wildland Fire 28, 750–760. https://doi.org/10.1071/WF18181.
Wine, M.L., Cadol, D., Makhnin, O., 2018. In ecoregions across Western USA streamflow increases during post-wildfire recovery. Environ. Res. Lett. 13, 014010. https://doi.org/10.1088/1748-9326/aa9c5a.
Wu, J., Baartman, J.E.M., Nunes, J.P., 2021. Comparing the impacts of wildfire and meteorological variability on hydrological and erosion responses in a mediterranean catchment. Land Degrad. Dev. 32, 640–653. https://doi.org/10.1002/ldr.3732.
Yang, Q., Zhang, X., 2016. Improving SWAT for simulating water and carbon fluxes of forest ecosystems. Sci. Total Environ. 569–570, 1478–1488. https://doi.org/10.1016/j.scitotenv.2016.06.238.
Yang, J., Reichert, P., Abbaspour, K.C., Xia, J., Yang, H., 2008. Comparing uncertainty analysis techniques for a SWAT application to the Chaohe Basin in China. J. Hydrol. 358, 1–23. https://doi.org/10.1016/j.jhydrol.2008.05.012.
Yang, Y., Hu, X., Han, M., He, K., Liu, B., Jin, T., Cao, X., Wang, Y., Huang, J., 2022. Post-fire temporal trends in soil properties and revegetation: insights from different wildfire severities in the Hengduan Mountains, Southwestern China. Catena 213, 106160. https://doi.org/10.1016/j.catena.2022.106160.
Zhang, H., Wang, B., Liu, D.L., Zhang, M., Leslie, L.M., Yu, Q., 2020. Using an improved SWAT model to simulate hydrological responses to land use change: a case study of a catchment in tropical Australia. J. Hydrol. 585, 124822. https://doi.org/10.1016/j.jhydrol.2020.124822.